AKENTEN APPIAH-MENKA UNIVERSITY OF SKILLS TRAINING

AND ENTREPRENEURIAL DEVELOPMENT

THE IMPACT OF MICROPILLAR DIMENSIONS OF AN N-ZNO/P-ZNTE SOLAR CELL USING FDTD SOLVER

(MTECH ELECTRICAL AND ELECTRONICS ENGINEERING)

MOHAMMED AKARIBOR YAKUBU

NOVEMBER, 2023

THE IMPACT OF MICROPILLAR DIMENSIONS OF AN N-ZNO/P-ZNTE SOLAR CELL USING FDTD SOLVER

(MTECH ELECTRICAL AND ELECTRONICS ENGINEERING)

MOHAMMED AKARIBOR YAKUBU

(7201200015)

A DISSERTATION SUBMITTED TO THE SCHOOL OF GRADUATE STUDIES, AKENTEN APPIAH-MENKA UNIVERSITY OF SKILLS TRAINING AND ENTREPRENEURIAL DEVELOPMENT, IN PARTIAL FULFILMENT OF THE REQUIREMENTS FOR AWARD OF THE MASTER OF TECHNOLOGY IN ELECTRICAL AND ELECTRONICS ENGINEERING DEGREE

NOVEMBER, 2023

DECLARATION

CANDIDATE'S DECLARATION

I, MOHAMMED AKARIBOR YAKUBU declare that this dissertation, with the exception of quotations and references contained in published works which have all been identified and duly acknowledged, is entirely my own original work, and it has not been submitted, either in part or whole, for another degree elsewhere.

MOHAMMED AKARIBOR YAKUBU

SIGNATURE: …….

DATE: …….

SUPERVISOR'S DECLARATION

I hereby declare that the preparation and presentation of the dissertation work was supervised in accordance with the guidelines on supervision of dissertation work laid down by the Institute of Education, Akenten Appiah-Menka University of Skills And Entrepreneurial Development.

ENGR. PATRICK NYAABA AYAMBIRE

SIGNATURE: …….

DATE: …….

ACKNOWLEDGEMENT

I want to sincerely thank Engr. Patrick Nyaaba Ayambire for continuing to support the entire research project at AAMUSTED. I also owe a huge debt of gratitude to Dr. Rabiu Musah Bilsi for his encouragement and assistance both before and throughout my graduate studies. Special thanks to Jonathan Afrifa, Maxwell Kwabena and Maxwell Babilo Banu; who has helped me in all conceivable manner that they could. Without them, it would not have been possible. I also want to express my gratitude to Dr. Albert Awoppone, my postgraduate coordinator, for his advice and support throughout the entire time I studied for this program. I am grateful to my colleagues at AAMUSTED for their concern and assistance. Also, I want to express my sincere appreciation to my family, who has always helped me out. The support of my family has always been the biggest inspiration for me to advance in my career. I've had the opportunity to encounter variety, meet lots of people, and learn from brilliant lecturers and experts from many professions thanks to AAMUSTED. Their perspectives and experiences have greatly influenced my decision to pursue further graduate studies there.

DEDICATION

I dedicate this to my family and friends.

TABLE OF CONTENT

LIST OF TABLES

TABLES **PAGES**

LIST OF FIGURES

FIGURES **PAGES**

ABSTRACT

This dissertation presents a study of three-dimensional (3D) cylindrical periodic micropillar solar cell structures made of negatively doped zinc oxide (n-ZnO) and positively doped zinc telluride (p-ZnTe). The impact of several variations in the dimensions including height, diameter/thickness and pitch of the axial and radial types of pillars has been conducted using Finite-Difference Time-Domain (FDTD) Solver in the Ansys Lumerical DEVICE Simulator software. Their analysed optical properties such as transmission, reflection and absorption indicate that the ZnO/ZnTe micropillar solar cells exhibit greater light absorption than planar ZnO/ZnTe solar cells of equal height, with a difference of roughly twelve percent (12%). They also exhibit a significant reduction in light reflection over the whole wavelength range. On the height variation, the highest degree of absorption was achieved by an absorber height of 1.0 µm (about 20%), an emitter height of 0.5 µm (also about 20%) for the axial junction micropillar; whiles the radial (core-shell) pillar height of 1.3 µm achieved more than fifty percent (50%). A pillar diameter / thickness of 240 nm leads to the highest level of absorption of about forty percent (40%) for axial diameter and about sixty percent (60%) for radial shell both within the wavelength 0.30 µm to 0.55 µm of the relevant spectrum. Whiles the radial core thickness of 140 nm attained the maximum absorption of about forty percent (40%). As for the pitch, we observe a non-monotonic response. The optimum zone has been identified at the extreme values of 0.3 µm and 0.7 µm. These findings imply that the ZnO/ZnTe combination is also promising for making solar cells with micropillars structure.

CHAPTER ONE

INTRODUCTION

1.1 Background

The global energy demands from the era of industrial revolution have so far been met using primarily fossil fuels such as coal, oil and gas. However, global concerns about rapidly rising carbon dioxide (CO_2) emissions in the atmosphere; depletion of fossil fuel (Coal, Oil, and Gas) reserves; geopolitical and military conflicts (like the Russian – Ukraine War); constant fuel price fluctuations, and the greenhouse effect and its resulting dramatic changes in global surface temperature and climate must be addressed as soon as possible. If these issues are not addressed, they will eventually result in unsustainable situations, posing a potentially irreversible risk to human existence (UNFCC, 2015).

One core aspect of the solution will be a speedy transition from the antiquated fossil-based energy system to a sustainable hundred percent (100%) renewable energy system (Tiwari & Mishra, 2012). This is undeniably a major driving force behind the development and implementation of high-efficient renewable energy technologies like solar cells.

1.1.1 Renewable Energy

Renewable energy refers to energy obtained from natural resources that are renewed more quickly than they are used up (Nations, 2022). Some sources of renewable energies are hydro-power, geothermal, ocean energy, wind, biomass, solar, etc. These sources with regards to their contribution to the world's energy demand, have not yet reached a level where they can be compared to fossil fuels. However, the global transition to renewable energy is increasing.

The German Advisory Council on Global Change's (WBGU) world energy vision 2100 (WBGU, 2003) predicts solar energy, including photovoltaics to emerge as a significant energy source. They are expecting it to account for about 20% of all global energy in 2050 and about 70% of total global energy in 2100 as illustrated in Figure 1.1 below.

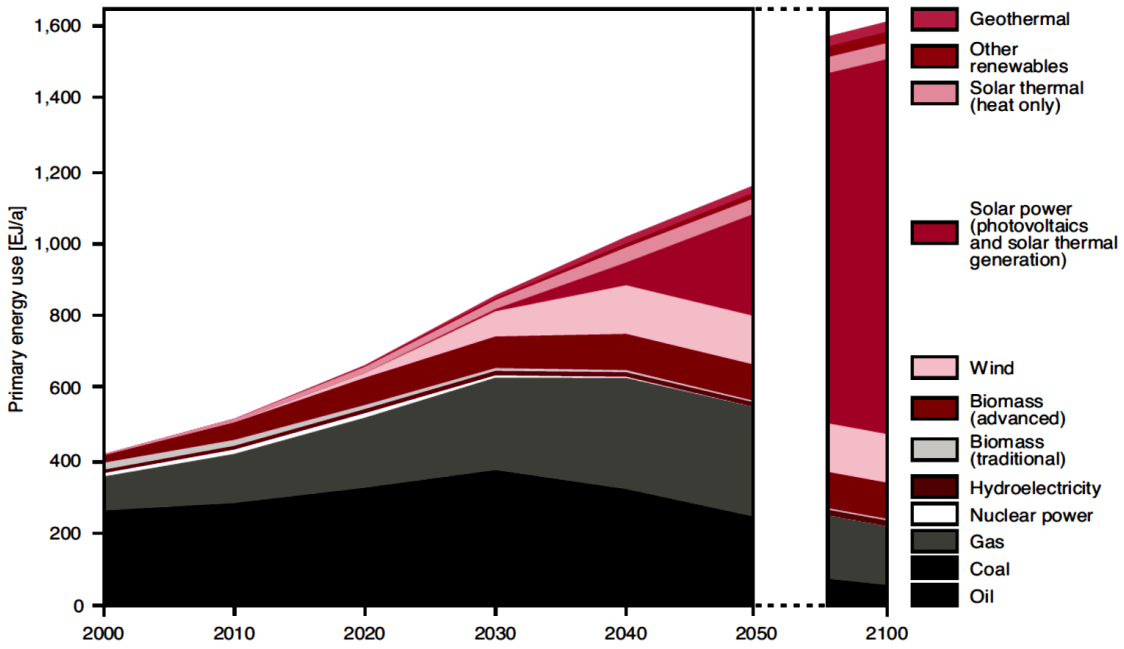

Figure 1.1: The energy mix for the world until 2050/2100 (WBGU, 2003).

This ambition can therefore become a reality by continuously advancing the science and technology of solar cells. That is, significant improvement is required in conversion efficiencies and dependability, as well as cost reductions for solar cells and modules.

1.2 Problem Statement

The conventional first-generation solar cells achieved twenty-six percent (26%) efficiency, are made with crystalline silicon (c-Si) (NREL, 2019). Although crystalline silicon can achieve better efficiency, the input required to synthesize highly purified silicon will accounts for almost 40% - 50% of the cost of a completed silicon-based module (Schrier, Demchenko & Alivisatos, 2007). Hence, it is not cost effective.

Meanwhile, the major component of solar cells, silicon (Si), is also in significant demand globally in other semiconductor-related industries, including computer chip design, analog electronics, and digital memory. As a result, unique structural designs and new material systems are being introduced to optimized solar cells.

A zinc oxide material has exhibited good thermal conductivity, high electron mobility, wide and direct bandgap. These characteristics has made zinc oxide (ZnO) unique and suitable for solar applications (Luo, He, Shen, Li, Yin, Oron & Lin, 2017). However, zinc oxide alone has several limitations in solar cell applications because, it is natively n-type, and producing p-type zinc oxide is extremely difficult (Fan, Sreekanth, Xie, Chang, & Rao, 2013). As a result, creating a p-n junction with just zinc oxide is difficult. Nonetheless, the ZnO-based homojunction solar cell has been demonstrated (Li, Zhai, Bando, & Golberg, 2012). The difficulty has to do with the large band-gap of zinc oxide (ZnO) which only enables the homojunction solar cell to primarily absorbs ultraviolent radiation with very little visible light (Liu, Sakurai, & Aono, 2010). Furthermore, bulk zinc oxide's (ZnO) maximum theoretical efficiency is just seven percent (7%) (Schrier et al., 2007).

One intriguing suggestion for lowering the high 3.3eV zinc oxide (ZnO) bandgap is to add certain additional materials, like zinc telluride (ZnTe) or zinc sulphide (ZnS) (Schrier et al., 2007). To address these constraints, the group II-VI material such as zinc telluride (ZnTe) could be mixed in a heterojunction arrangement with zinc oxide (ZnO) (Schrier et al., 2007).

Zinc telluride (ZnTe) material is inherently p-type due to the fact that its deficiencies, including zinc vacancies, are located inside the valence band instead of the bandgap. As a result, zinc telluride may be readily combined with zinc oxide to produce a p-n junction.

Interestingly, high photo-response in n-ZnO/p-ZnTe solar cells has been recorded between 2.3eV to 3.6eV (Wang, Lin, & Phillips, 2008).

Even after several innovations, solar cells continue to face challenges in terms of high efficiency and cost reduction. This work focuses on group II=IV materials which have not been thoroughly explored and are not environmentally hazardous.

1.3 Objectives

The aim of this work is to simulate, optimize and analysed innovative solar cells constructed with safer semiconductors from group II to group VI materials. The specific objectives of this research include to:

1. perform a comparative analysis of the safer II-VI semiconductor materials based micropillar solar cell and the planar solar cell.
2. analyse the effects of physical parameters on the proposed micropillar solar cell

1.4 Significance of the Study

This dissertation will contribute to existing research and development efforts in the field of solar cell structure and designs. It will also suggest a feasible idea for developing a cost-effective and environmentally friendly solar cell. Since p-n junction allows for better light scattering and trapping by orthogonalizing the direction of light absorption and charge separation (Garnett & Yang, 2010); this work will show the potential of microstructure p-n junction in improving device efficiency.

1.5 Dissertation Outline

The first chapter gives a quick overview of the fundamental ideas behind solar cell functioning, along with information on the various varieties and performance metrics. It

also covers the fundamentals of micropillar solar cells and offers justification for the application of the ZnO/ZnTe material combination.

The chapter two present a critical evaluation of the state-of-the-art in the area of ZnO/ZnTe solar cells. The chapter also highlights the hypotheses and evidence of ZnO/ZnTe solar cells as well as the effects of various micropillar dimensions.

Chapter three present the simulation's setup and input variables utilized for this project, as well as the optical and electrical characteristics of zinc oxide (ZnO) and zinc telluride (ZnTe). It also presents an analysis of several device varieties of ZnO/ZnTe solar cells including axial, radial, and planar structures.

The fourth chapter discusses the findings of the performance study of the ZnO/ZnTe micropillar solar cell, along with an analysis of the effects of pillar length, thickness/diameter and pitch.

The last chapter, chapter five, offers summaries, conclusion and future outlook of this research.

CHAPTER TWO

LITERATURE REVIEW

In this chapter a review of the literature in regards to ZnO/ZnTe based nanopillar solar cell's dimensions on its generation rate and current were reviewed.

2.1 Zinc Oxide Solar Cells

Solar cells made with zinc oxide (ZnO) materials are essential because of its high conductivity, strong electron affinity, exceptional electron mobility and its stability (Wibowo, Marsudi, Amal, Ananda, Stephanie, Ardy, & Diguna, 2020).

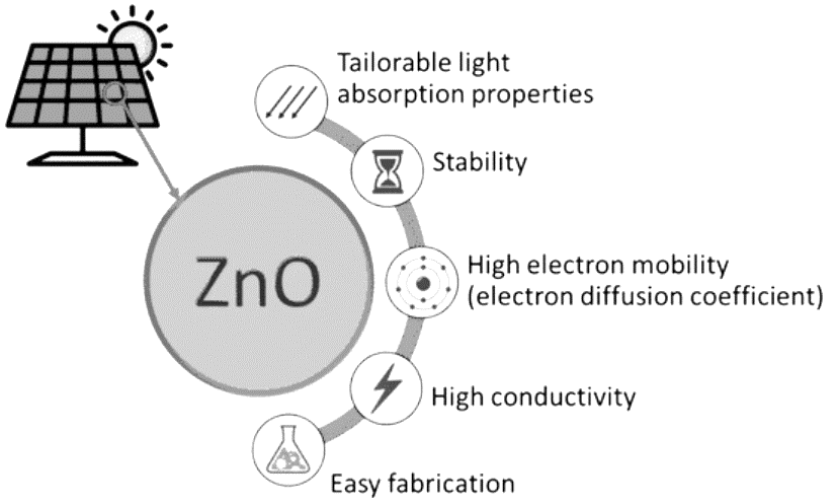

Figure 2.1: Illustration of the advantages of zinc oxide (ZnO) (Wibowo et al., 2020).

An organic solar cell with a 2.7% maximum efficiency of power conversion was created by Takanezawa, Hirota, Wei, Tajima, & Hashimoto, (2007), using a ZnO nanorod array with controlled dimension. The hydrothermal procedure used in this study to fabricate the nanorods produced an array of nanorods with a 20–40nm diameter and a height of 0.3mm long. This research led to the conclusion that the effectiveness of the device is significantly influenced by the length of the nanorod and the thickness of the organic

layer, with performance improving as the average nanorod length increased. Sakai, Usui, & Murakami, (2013), also investigated the relationship between the size of zinc oxide (ZnO) particles in porous semiconductor electrodes and their photovoltaic efficiency in dye-sensitized solar cells (DSSCs). The DSSCs with ZnO particles size of 40*nm* showed the highest power conversion efficiency among those with particles ranging in size from 20*nm* to 2μm.

Vittal & Ho, (2017) proposed the addition of dopants as one technique of improving electron transport to enhance the efficiency of ZnO solar cells. The dopants fill the cell's holes, increasing the number of electrons injected in the semiconductor for recombination. In terms of doping, (Lanjewar & Gohel, 2017) doped ZnO with silver (Ag), and observed that the band gap of the resultant silver doped zinc oxide (Ag:ZnO) got drastically reduced from 3.28*eV* for pure ZnO to 2.65*eV* for Ag:ZnO. This resulted into an increase of ZnO solar cell's power conversion efficiency from 0.55% to 2.02%. due to the absorption of large amount of visible light by the Ag:ZnO photoelectrode.

Also, (Mahmood & Park, 2013) reported that a solar cell fabricated with boron-doped zinc oxide (B-ZnO) nanosheets had a considerable increase in power conversion efficiency of 6.75% over undoped zinc oxide (ZnO) nanosheets of 2.62%; and according to research by Goel and his colleagues, a lanthanum-doped zinc oxide (La-ZnO) based nanopowder solar cell outperformed the pure ZnO based solar cell in terms of photovoltaic performance. Its light harvesting efficiency rose from 0.20% to 0.36% after doping it with lanthanum (La) (Goel, Sinha, Yadav, Joseph, & Kumar, 2017).

ZnO in the form of nanoparticles can be used as a substitute for ZnO thin film in solar cell configurations. (Zang, 2018), demonstrated this by using a perfectly oriented, micrometre grain-sized Cu2O/ZnO thin film to fabricate a solar cell with a power

conversion efficiency of 3.17%. Later, he replaced the ZnO thin film with ZnO nanoparticles in a similar setup, but this time using lead (II) sulphide (PbS) quantum dots nanocrystals as the p-type material. The power conversion efficiency of the resultant solar cell almost double that of the planar ZnO cell (η = 2.94%). Jouane, Colis, Schmerber, Kern, Dinia, Heiser & Chapuis, (2011), performed radio frequency magnetic sputtering to deposit a ZnO layer over the active layer of a typical organic solar cell. The ZnO layer deposition caused no functional damage to the photoactive layer and increased the cell efficiency from 2.16% to 2.34%.

In terms of ZnO heterojunction solar cell, Leschkies, Beatty, Kang, Norris, & Aydil, (2009) discovered that in comparison to thin films, nanostructures have a higher interfacial area for exciton dissociation, and hence anticipated an improved overall device performance. They advocated using nanostructures instead of flat sheets to improve efficiency. Beek, Wienk, & Janssen fabricate a bulk heterojunction solar cell using separately manufactured nanocrystalline ZnO with a diameter of ~5*nm*. This arrangement achieved a power conversion efficiency of 1.6% at 0.71 sun equivalent intensity and was generally constant at 1.7 sun equivalent intensity (η = 1.4%). In a comparable arrangement, the forward current density in the cell with ZnO was considerably greater than in the cell without ZnO, demonstrating that the presence of nanocrystalline ZnO does indeed offer a continuous channel for electron transport (Beek, Wienk & Janssen, 2004).

Olson, Piris, Collins, Shaheen & Ginley, (2006), demonstrated the concept of using vertically aligned ZnO nanofibers in conjunction with a polymer (P3HT) to produce a heterojunction solar cell device with a power conversion efficiency of 0.53%. The modest findings according to (S.-S. Li & Chen, 2013) were due to be the consequence of

numerous unoptimized parameters, including the spacing between ZnO nanofibers (100*nm*), which is excessively big in comparison to the normal exciton diffusion length in P3HT (10-20*nm*), resulting in inefficient charge separation.

According to Gharghi, Fathi, Kante, Sivoththaman & Zhang, (2012) study, vertical aligned type-II hetrojunction core/shell micropillars structures may be used in solar cells due to their greater surface-to-volume ratio, stronger light-trapping effect, and a longer carrier lifespan than planar structures. In a similar demonstration, Akram, Javed, Islam, Mujahid & Safdar, (2016), used Al-doped ZnO/ZnSe core/shell nanorod arrays grown from ZnO seed layer to produce a solar cell with an efficiency of 2.2%. This is a significant increase over a solar cell with a similar design employing planar ZnO and ZnS as a buffer layer ($\eta = 0.16\%$).

Despite several evidence of progress achieved in ZnO development so far, there is still plenty room for further advancement. In order for ZnO to be more competitive in solar cell applications, it must have a larger surface area and better light-harvesting capabilities. These enhancements would result in greater power conversion efficiency and a longer lifetime in a variety of situations with varying heat conditions, humidity, and mechanical loads.

2.2 Zinc Telluride Solar Cells

Zinc telluride (ZnTe) is one of the most promising II-VI semiconductor alternatives for the manufacture of low-cost, and highly efficient solar cells (Han, Choi & Park, 2003). This is attributed to its large band gap of 2.23-2.28*eV* at room temperature (Fang, McCandless & Opila, 2009), which can serve as a back contact for thin or fully depleted device structures (Sites & Pan, 2007); high absorption coefficient of close to $10^5 cm^{-1}$,

and low electron affinity of 3.73eV (Pistone, Arico, Antonucci, Silvestro & Antonucci, 1998). Finally, ZnTe can be strongly doped ($>10^{20}cm^{-3}$) (Gessert, Mason, Reedy, Matson, Coutts & Sheldon, 1995); to create an efficient tunnel junction to the metal layer (McCandless & Dobson, 2004). Additionally, ZnTe is a p-type semiconductor that may create a p-n junction with an n-type layer, making it more useful for the photovoltaic conversion of solar energy.

The commercial modules produced by First Solar Inc., incorporated ZnTe buffer layers into it (Strevel, Trippel, Kotarba & Khan, 2013). Their device's efficiency, as well as the stability and temperature sensitivity of their modules, have all been said to have improved with the addition of ZnTe. Using Solar Cell Capacitance Simulator Software (SCAPS), numerically simulated a modelled solar cell based on zinc telluride (ZnTe) thin film as the active absorber Skhouni, El Manouni, Mari & Ullah, (2016).

In order to achieve the ideal ZnTe film thickness, a thorough study of the impact of ZnTe absorber thickness on a number of operating parameters, including open-circuit voltage Voc, short-circuit current density Jsc, fill factor FF, and photovoltaic conversion efficiency, was conducted. It reveals that increasing the thickness of the ZnTe absorber layer leads to a better efficiency until a maximum value is reached and thereafter marginally declines. This maximum value was discovered to be 10% of ZnTe optimum thicknesses close to 2μm. Tanaka, Miyabara, Saito, Guo, Nishio, Yu & Walukiewicz, (2013); investigated on the impact of n-type layer thickness on photovoltaic characteristics by varying the thermal diffusion time. They obtained a conversion efficiency of 0.78% when a 200nm-thick n-ZnTe layer was used. However, due to the poor crystalline quality of the n-ZnTe layer, the efficiency was considerably low when compared to the value calculated for a single-junction ZnTe solar cell.

2.3 Zinc Oxide / Zinc Telluride Solar Cells

Luo, He, Shen, Li, Yin, Oron & Lin, (2017) used well-aligned type-II nanowire arrays to fabricate a ZnO/ZnTe core-shell solar cell structure. The process flow is described in Figure 2.2.

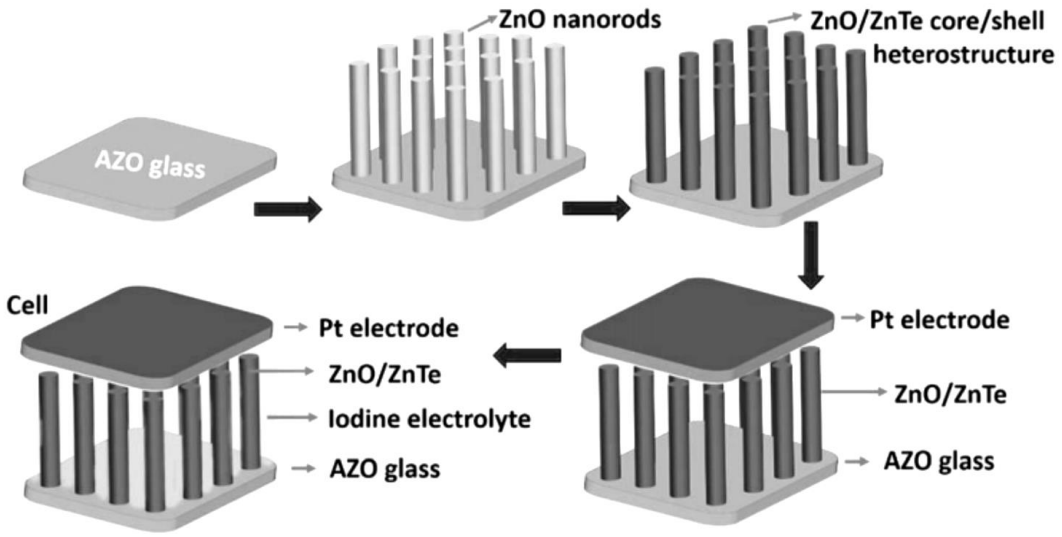

Figure 2.2: ZnO/ZnTe heterostructure-based solar cell with vertical alignment. ***(Luo et al., 2017)***

They examined the morphology, size distribution and optical properties of the ZnO/ZnTe core-shell nanowire arrays transmission measurement. Their report indicated that the ZnO/ZnTe core-shell nanowire arrays have good light absorption characteristics making it suitable for making photovoltaic applications.

Kabalan & Sohid, (2020), performed numerical analysis using Lumerical's Finite Difference Time Domain (FDTD) solver to investigate the effects of doping level in the absorber layer. Based on the range of parameters analyzed, they concluded that for a core-shell ZnO/ZnTe micropillar solar cell of 4μm height, 0.5μm pitch, and 70nm shell thickness with a $2.16\times10^{19} cm^{-3}$ doping concentration for ZnTe achieves an efficiency of 17%.

Shaygan, Davami, Jin, Gemming, Lee & Meyyappan, (2016) described the fabrication and characterization of a field effect transistor with a radial core/shell configuration based on ZnTe nanowire. They tune the shell to core ratios in integrated devices successfully and where able to control the electrical and photoconductive performance of the devices. They found that the ZnO shell around the ZnTe nanowire has a considerable influence on the optical characteristics of the transistor, increasing the photo-to-dark current ratio, responsivity, and photoconductive gain to 199, 196, and 8.12×10^{4}% respectfully for the 17.5% shell/core ratio. Their ability to alter the core/shell ratio demonstrated here is encouraging in device design for optoelectronic applications requiring a broad range of wavelengths.

Chao, You, Lu, Cheng, Chang, Liang & Wu, (2011) produced a vertically aligned ZnO/ZnTe core-shell nanowires on a plane sapphire substrate. Their nanowires exhibited good optical qualities, as evidenced by three-dimensional fluorescence pictures acquired with a laser scanning confocal microscope. Electrical tests also show that the p-type ZnO/ZnTe field-effect transistor device has a switch on voltage of 1.65V and a hole mobility of 13.3$cm^2/V\,s$.

Chao, Cheng, Lu, Chang, Cheng & Chen, (2010) created type-II ZnO/ZnTe core-shell nanowire arrays with large areas and excellent alignment on a plane sapphire substrate. They used Scanning Electron Microscopy (SEM) to analyze the shape and size distribution of the ZnO/ZnTe core-shell nanowire arrays, and the optical properties were investigated using transmission measurement. Their results showed that the ZnO/ZnTe core-shell nanowire arrays had high crystalline quality. Furthermore, it was discovered that the nanowire arrays exhibit high light absorption qualities, making them appropriate for the fabrication of photovoltaic systems.

Enhancing carrier transport is crucial for improving semiconductor device performance. Xu, Lee, Bell, Smith, Zhang, Ju, Chen & Pan, (2010) investigated carrier transport mechanisms in nanojunctions made up of vertically aligned ZnO nanostructures and a ZnTe matrix using theoretical and experimental methods. They efficiently distributed and gathered carriers across the nanostructure without trapping them in the p-n regions. Also, because the structure was designed to be entirely depleted, the nanocone junction demonstrated improved carrier transport capabilities.

Wang, Lin & Phillips, (2008) grew heterojunction diodes with n-type ZnO and p-type ZnTe on GaAs substrates. They detected a high photoresponse in the energy range of $2.3eV$ to $3.6eV$, which corresponds to the bandgap energies of ZnTe and ZnO, respectively. They also observed a photovoltaic response with a short-circuit current of $0.8mA/cm^2$ and an open-circuit voltage of $60mV$ under tungsten lamp illumination. They believed that the imperfections due to the mismatch between the ZnTe and ZnO structures, as well as defects in the ZnO layer deposited at low temperature restricted the photovoltaic response.

2.4 Micropillar Solar Cells

Baytemir, Ciftpinar & Turan, stated that micropillar solar cells are cells constructed with high density array cylindrical pillars. Unlike planar cells, radial junction micropillars provide carrier collecting paths that are separate from the direction of photon absorption. While photons are usually absorbed along the pillars' heights, photogenerated carriers are mostly gathered in the radial direction. They also outperforms planar junction solar cells in terms of surface reflectance and light trapping (Baytemir, Ciftpinar & Turan, 2019). From an optical perspective, vertically arranged pillars exhibit

considerable broadband absorption (Kelzenberg, Boettcher, Petykiewicz, Turner-Evans, Putnam, Warren, Spurgeon, Briggs, Lewis, & Atwater, 2010).

According to Um et al. (2015), radial p-n junction structures with vertically aligned micropillar arrays enable the fabrication of solar cells with short minority carrier diffusion lengths. Due to the harvesting of photogenerated carriers with little recombination, this property permits the use of low-quality materials with high defect density and contaminants.

The combined structure of silicon micropillar with Cu nanoparticles solar cell was studied by Zhang, Fan, Zhang, Ma, Jiang & Ma, (2018); and it achieved an efficiency of 11.5%. They found that the improved power conversion efficiency was partly attributable to bigger short circuit currents caused by increased light absorption and shorter carrier collecting length, with a considerable contribution from multiple reflection in the micropillar arrays.

Shieh, You, Liu & Chiu, (2016) investigated and reported on an approach for reducing micropillar surface reflection by merging micropillar and nanostructure to form a superstructure that enhances both electrical and optical qualities. They discovered that a 2% change in micropillar height lowered averaged reflection from 16.73% to 9.63% and increased efficiency from 9.26% to 9.62%.

Micropillars with smooth sidewalls were used to construct radial junction solar cells with varying micropillar lengths by Baytemir et al., (2019). Standard doping was carried out for the creation of the solar cells. They observed a significant decline in the reflectance values as the micropillar length increases, The short-circuit current density and efficiency in the solar cells rather tended to increase with micropillar length up to 11.5μm, and then

decreased due to increasing surface recombination. In this study, a maximum efficiency of 17.26% was attained.

Although there is a wide window for enhancing solar energy harvesting in terms of silicon nanowire diameter and array pitch, Kelzenberg et al., detected that increasing pillar diameter or period initially led to an increase in absorption efficiency for a constant diameter to period ratio, and then a decrease. The tendency, according to them, was caused by a compromise between increasing light reflection and light transmission suppression (Kelzenberg et al., 2010).

2.5 Summary

According to published research, ZnO is distinct from other II-VI materials in that it has a high electron mobility, a wide and direct bandgap, strong thermal conductivity, low resistivity, and is chemically compatible with ZnTe (Luo et al., 2017). In contrast to ZnO (3.3 eV), ZnTe exhibits a smaller bandgap of 2.23-2.29eV (Wang et al., 2008). As a result, ZnO/ZnTe shows a reduced effective bandgap and may thus absorb energy in the visible light spectrum (Chao et al., 2010). The ZnO/ZnTe structure is also promising for achieving a micropillar type solar cell. The surface area of the micropillar solar cell is increased by its geometric design (Mariani, Haddad, Rajagopal & Huffaker, 2022). The Shockley–Quiesser model predicts that ZnO/ZnTe quantum well heterostructures might achieve 30% efficiency (Schrier et al., 2007). The nontoxic and environmental nature of ZnO and ZnTe has also been established by (Chao et al., 2010).

CHAPTER THREE

MATERIALS AND METHODOLOGY

This chapter will provide a detailed description of the simulation framework; the physics-based principles of the simulation along with the solution mechanism; and the simulated properties of the ZnO/ZnTe solar cell.

3.1 Ansys Lumerical

This study employs a simulation-based technique to numerically examine the desired input parameters of an array of three dimensional (3D) cylindrical micropillar structured ZnO/ZnTe solar cell. The three-dimensional (3D) Finite Difference Time Domain (FDTD) algorithm of the Ansys Lumerical's DEVICE Multiphysics Simulation Suite v2020 R2.4 software is used.

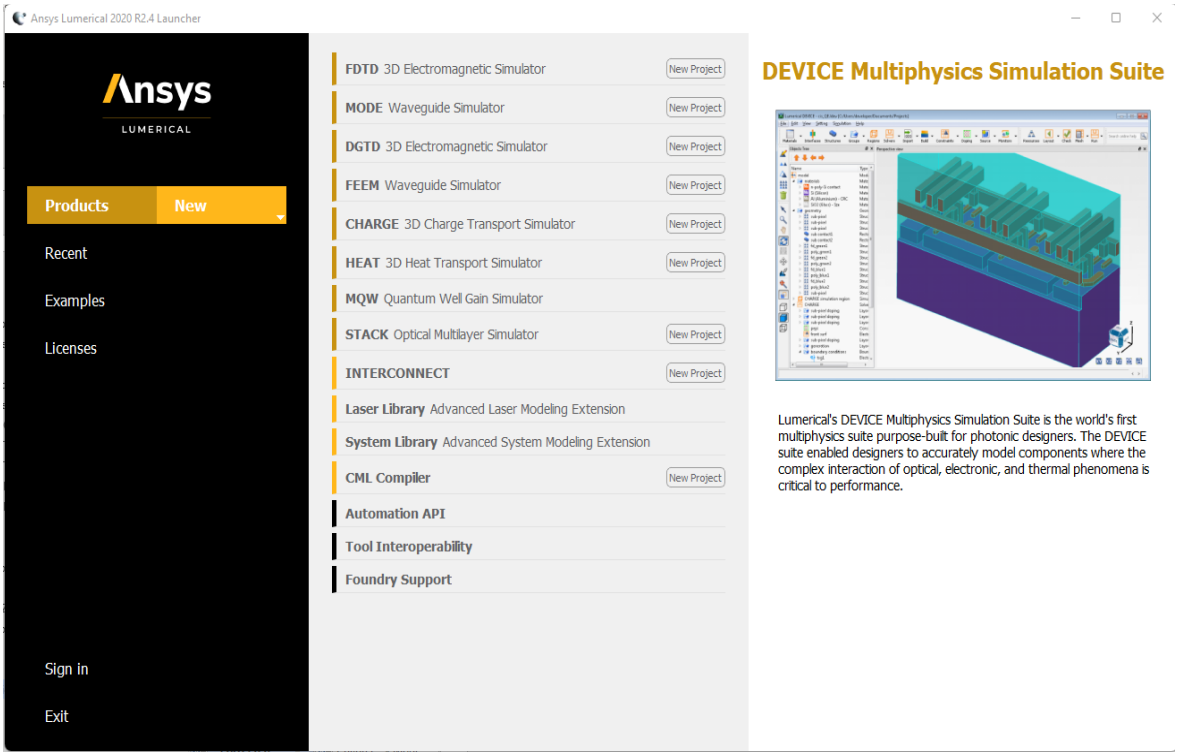

Figure 3.1: Ansys lumerical launcher

The software solves Maxwell's equations for arbitrary complex geometries when no analytical approach for predicting photonic device light behavior exists. It is also ideal for mimicking devices with feature sizes of a wavelength or less, and it yields a broadband result in a single simulation (*Trusted Photonic Simulation Tools - About Lumerical*, year.). Greulich, Fellmeth, Glatthaar, Biro & Rein, stated that the simulation method has already been used to explain our current understanding of solar cell devices, and it will be required for future device enhancements (Greulich, Fellmeth, Glatthaar, Biro & Rein, 2012).

3.2 Structures of Device Models

In this study, two alternative geometrical shapes of solar cells were studied. The first is a planar structure, and the second is a cylindrical pillar structure. Exploration of microstructures or nanostructures such as micropillars, nanorods, and quantum dot structures is rapidly increasing in the scientific community due to their high efficiency and low-cost capabilities (Dhar, Pradhan & Roy, 2016).

3.2.1 Planar ZnO/ZnTe Solar Cell Structure

In the planar shape ZnO/ZnTe solar cell shown in Fig. 3.8, ZnO is the emitter layer and ZnTe is the absorber layer. They are both placed on an aluminium (Al) doped zinc oxide (ZnO) transparent metal oxide substrate (AZO).

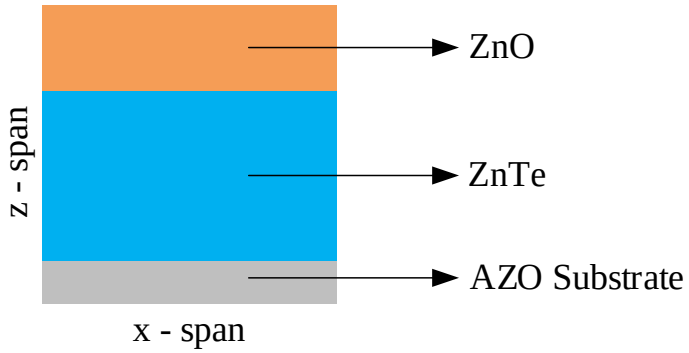

Figure 3.2: Planar solar cell structure

AZO has higher stability, is more abundance and is less expensive compared with the most popular transparent conductive oxide, indium tin oxide (ITO) which is highly toxic and scarcer (Wang et al., 2011).

3.2.2 Micropillar Solar Cell

The pillar structure provides potential benefits over the planar form in terms of light reflection, light trapping, bandgap tuning, and defect tolerance (Garnett, Brongersma, Cui & McGehee, 2011). Manufacturing development has also advanced dramatically over the years, increasing the capability of producing these high-performance electronic devices. Micropillar solar cells are categorized into axial and radial structural types on the basis of their formation of the p-n junction (Sahoo & Kale, 2019). The p-n junction determines the collection of the generated charge carriers.

3.2.3 Axial Junction ZnO/ZnTe Solar Cell

The axial junction type of micropillar solar cell reduces light reflection and increases light trapping possibilities. As a result, the pillars may be made as big as feasible (to absorb more light) without negatively impacting collecting efficiency. Therefore, pillar dimension adjustment may improve the properties of light absorption and light trapping.

A cross-sectional view of a single pillar from an axial junction ZnO/ZnTe micropillar solar cell is shown in Figure 3.3 below.

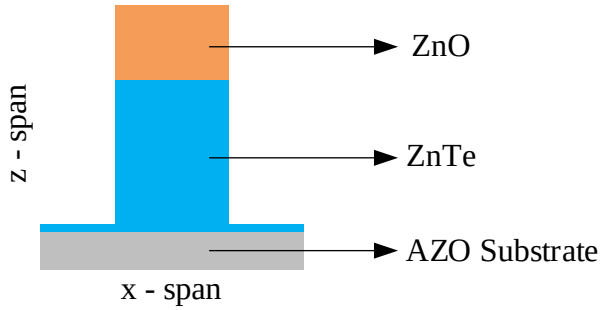

Figure 3.3: Single pillar of an axial p-n junction

The pillar's bottom (blue portion) is composed of ZnTe material, while the top (orange portion) is composed of ZnO.

3.2.4 Radial Junction ZnO/ZnTe Solar Cell

In the radial junction ZnO/ZnTe solar cell, the direction of incident light and carrier collection are orthogonal. As a result, the pillars can be as long as needed to absorb all of the incident light, and the radius must be narrower than the minority carrier diffusion length to gather all of the created carriers. A cross-sectional view of a single radial (core-shell) junction of a ZnO/ZnTe micropillar solar cell is shown in Figure 3.4 below.

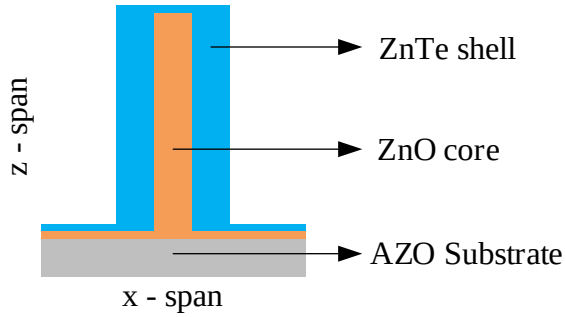

Figure 3.4: Single pillar of a radial (core-shell) p-n junction

The pillar consists of an outer ZnTe shell and an inner cylindrical ZnO core (blue and orange portions, respectively).

3.3 Simulation Framework

The Finite-Difference Time-Domain (FDTD) solver is used to study the impact of physical parameters (height, pitch, and diameter) on a three-dimensional (3D) micropillar ZnO/ZnTe solar cell's optical performance (reflection, transmission, and absorption).

3.3.1 Simulation Setup

The standard work flow is to first create the materials needed in the simulation, if the material data isn't already available from the default material database. Once the materials are defined, the structures and the FDTD simulation region are setups. The simulation region is where the boundary conditions, mesh, and simulation time are set. Next, sources are added to inject fields into the simulation region, and monitors are added to record data. These steps of the optical simulation process are depicted in the flow chart below.

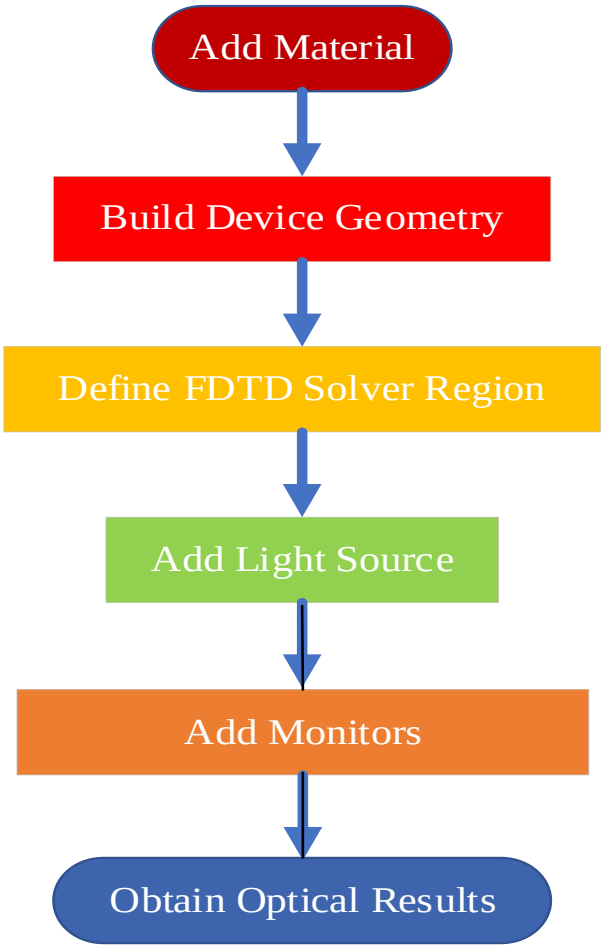

Figure 3.5: The steps for the optical simulation process of the Finite- Difference-Time-Domain

After the simulation is complete, the data can be accessed using standard functions like getdata, transmission, getelectric, etc.

3.3.2 Adding Material

The experimental data for ZnO and ZnTe is saved in a text file with three columns: the first column provides the wavelength or frequency, the second and third columns carry the real and imaginary parts of their refractive index (n, k). This is then imported into the material database as a new material. The fitting of the material is then adjusted with the help of the Material Explorer, using fit tolerance and max co-efficient parameters.

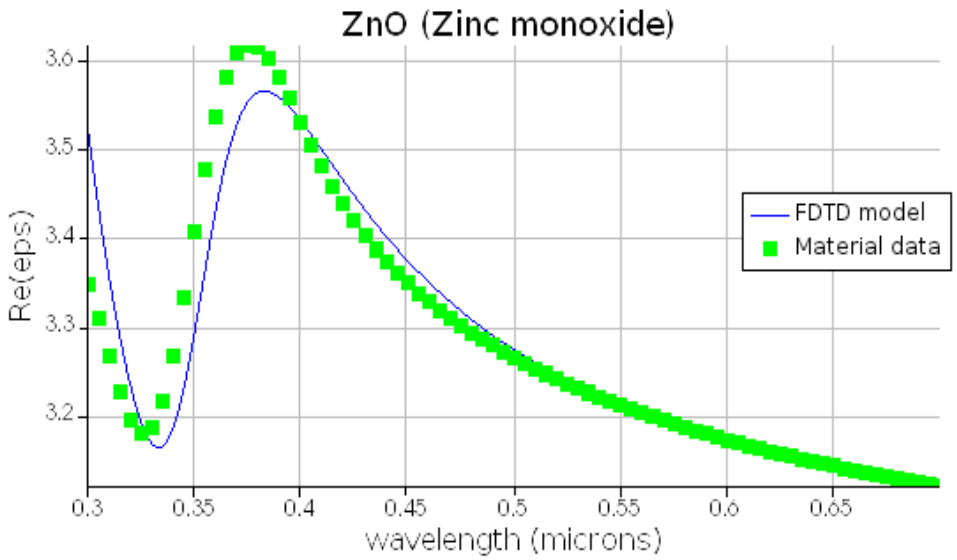

Figure 3.6: Fitting of real components (n) of the refractive index for ZnO with Material Explorer.

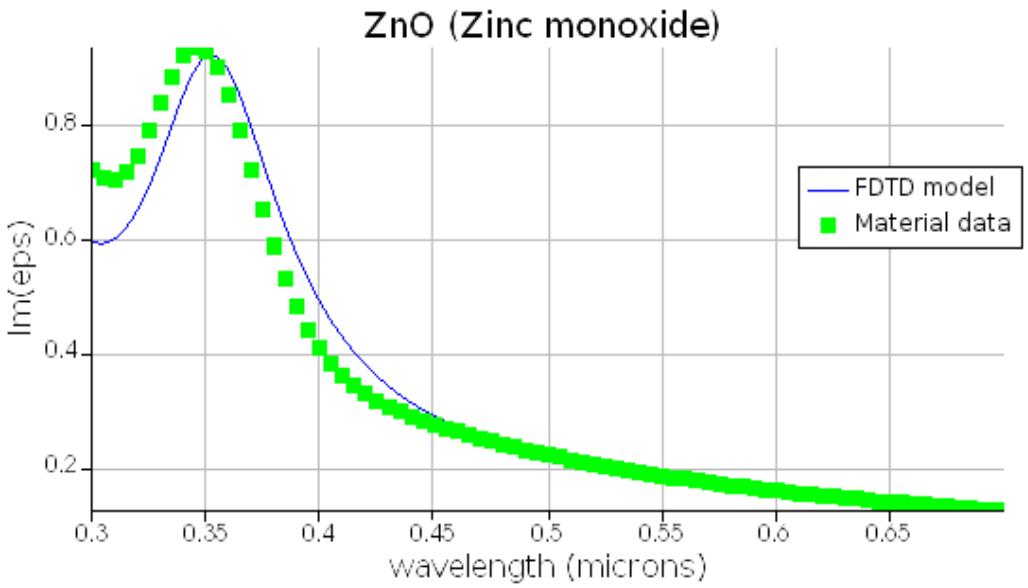

Figure 3.7: Fitting of imaginary components (k) of the refractive index for ZnO with Material Explorer.

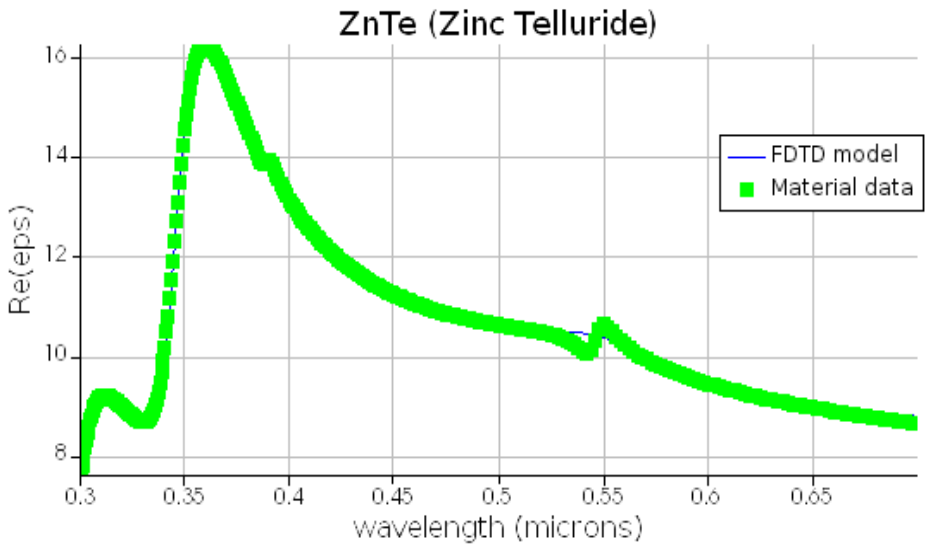

Figure 3.8: Fitting of real components (n) of the refractive index for ZnTe with Material Explorer.

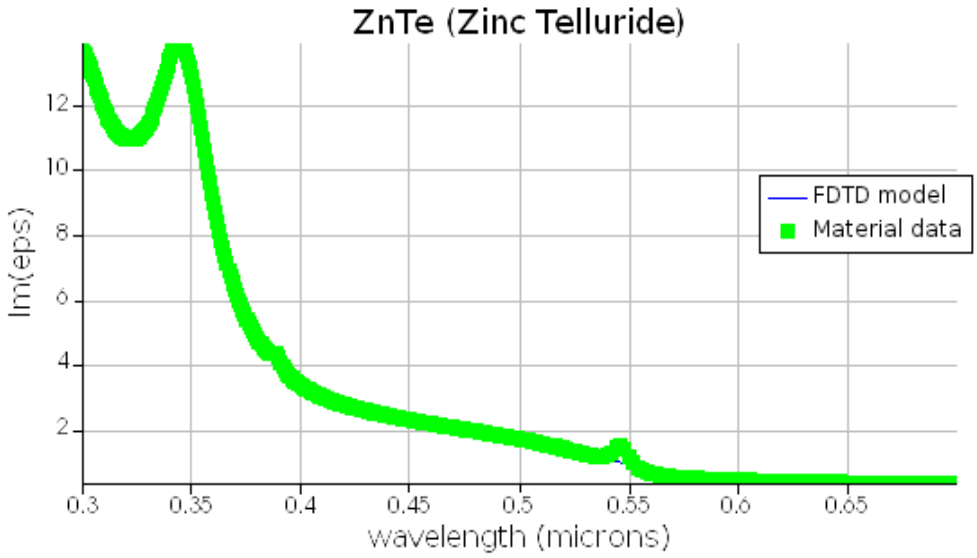

Figure 3.9: Fitting of imaginary components (k) of the refractive index for ZnTe with Material Explorer.

The blue curves represent outputs using the FDTD model, whiles the green curves represent the plots obtained using experimental (*n*, *k*) values.

3.3.3 Building Device Geometry

The device's whole construction is formed using predefined structures from the structure menu, such as rectangular, cylindrical, and triangular objects (Lumerical, 2019). The object library also contains some pre-built structures, which can be opened from the components button. The ZnO/ZnTe micropillars and planar solar cells employed in this study have all been constructed and placed on an Al-doped ZnO (AZO) glass substrate for the purposes of this investigation. The dimensions of the AZO glass substrate are x span = 5.0μm, y span = 5.0μm and z span = 1.0μm.

Planar Solar Cell

The standard ZnO/ZnTe structure consists of a 0.5μm emitter layer (ZnO) and a 1.0μm absorber layer (ZnTe).

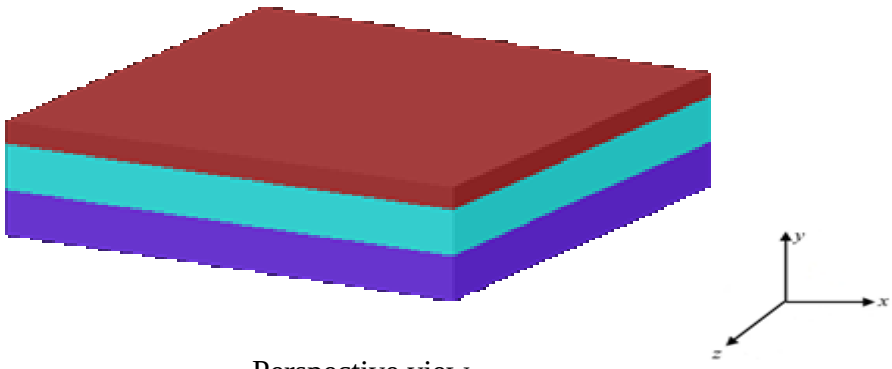

Perspective view

XY view XZ view YZ view

Figure 3.10: 3D schematic of planar ZnO/ZnTe solar cell.

Axial Micropillar Solar Cell

The axial junction ZnO/ZnTe follows the same geometric dimensions as planar structure except for its cylindrical pillar structure. The top part of the pillar is 0.5μm and the bottom part is 1μm which adds up to 1.5μm. The radii of both the top (ZnO) and bottom part (ZnTe) axial junction micropillar are set to 100 *nm*, which provides each of them with a pillar diameter (d) of 200*nm*.

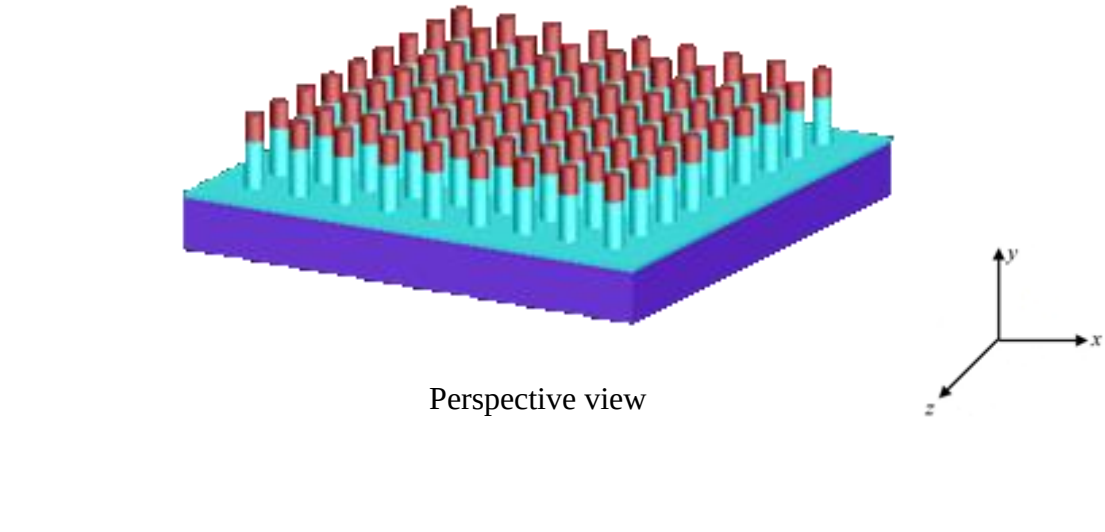

Figure 3.11: 3D Schematic of ZnO/ZnTe axial junction micropillar array solar cell.

Radial Micropillar Solar Cell

In the case of radial junction ZnO/ZnTe micropillar solar cell, the pillar height of both the core and shell are 1.5μm each. The radius of the core (ZnO) and thickness of the shell (ZnTe) of the core-shell ZnO/ZnTe micropillar are 50*nm* and 100*nm*, respectively.

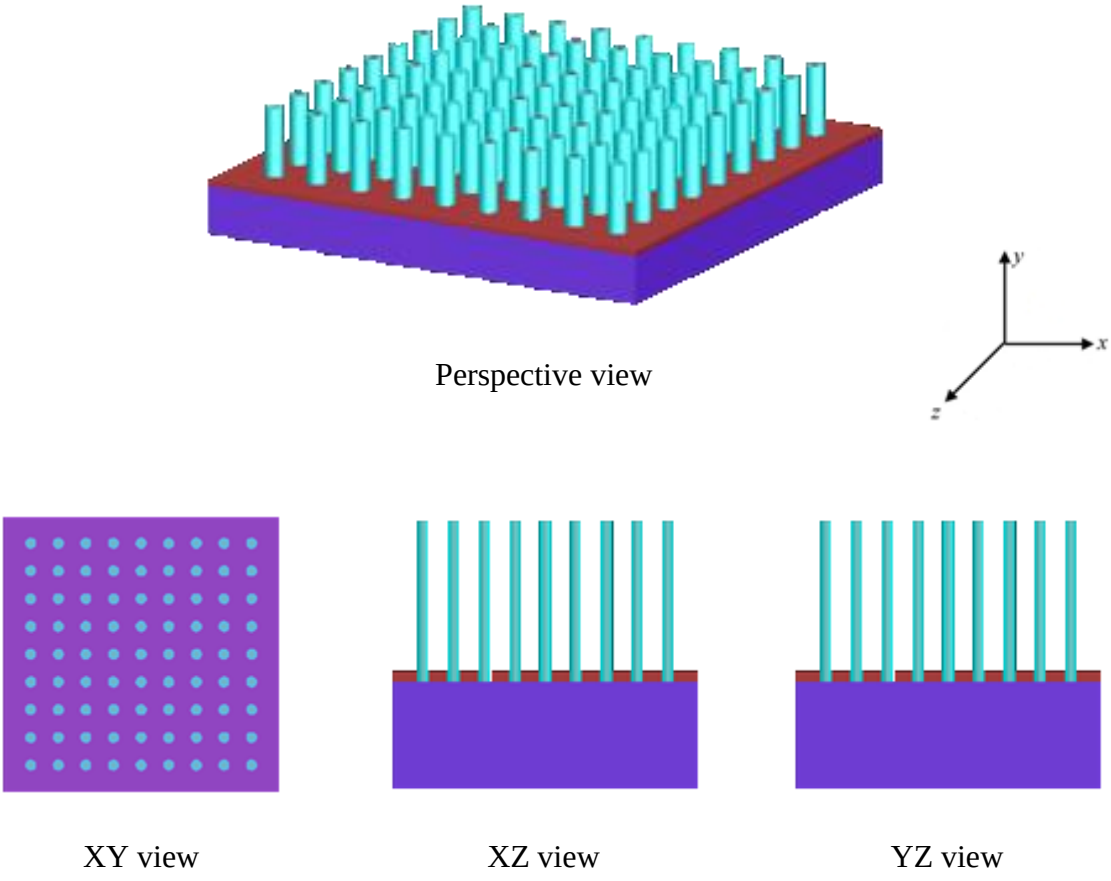

Figure 3.12: 3D Schematic of ZnO/ZnTe radial junction (core-shell) micropillar array solar cell.

The spacing between two pillars (pitch) is adjusted at 0.5μm for both axial and radial micropillars.

3.3.4 Solver Region

A periodic region is defined instead of solving the entire system under consideration. These will include defining the simulation time, boundary conditions, and mesh settings. One-unit cell (x span = 0.5μm, y span = 0.5μm and z span = 1.5μm) which contains a single pillar of the entire periodic micropillar structure delivers results for the entire device. The same or similar unit area is considered for the planar structure. The objects outside of the solver region are not part of the active computation. The selection of a

small portion from the entire system helps in reducing computation time and saves memory space. The mesh type is set to uniform, whiles all other settings are left default. The periodic boundary conditions are used on both the x and y boundaries. Perfectly Matched Layers (PLM) boundary condition is used on the z boundary to absorb incident light with minimal reflection.

3.3.5 Light Sources

A periodic plane light (or electromagnetic waves) source is injected in the z-axis at the position of 1.5μm within the simulation region as an input parameter to the system. The desired wavelength range used is 0.25μm to 0.65μm. The FDTD source will automatically inject a spectrum calculated from a Gaussian-like shaped pulse, as shown in the Frequency/Wavelength tab (screenshot below).

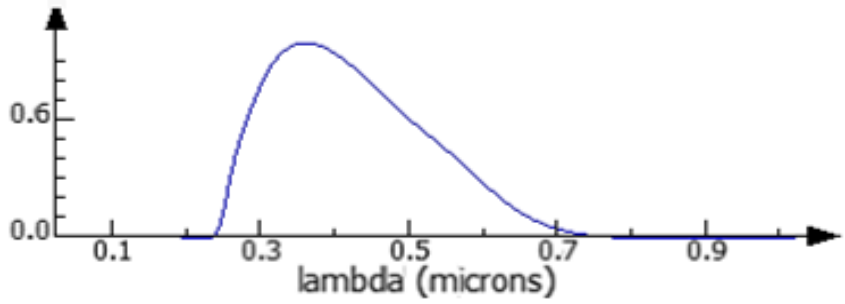

Figure 3.13: Spectrum verse wavelength of the source wave

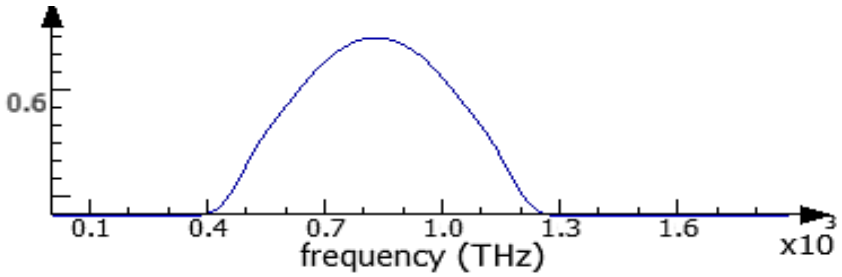

Figure 3.14: Spectrum verse frequency of the source wave.

The time domain is set to have a broadband pulse type with the following characteristics:

Table 3.1: The used broadband signal characteristics

Characteristic	Unit	Value
Frequency	Terahertz (THz)	830.194
Pulse length	Femtosecond (fs)	6.64572
Offset	Femtosecond (fs)	18.8428
Bandwidth	Terahertz (THz)	737.951

An advance option of eliminating discontinuities is selected to produce a time signal graph as shown in Figure 3.15 below.

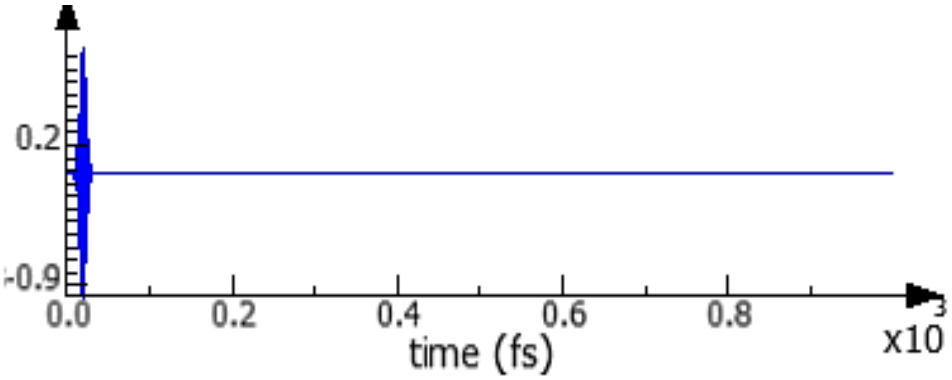

Figure 3.15: Signal verse time of the source wave.

3.3.6 Monitors

The frequency domain monitors are used to generate response of the device. By default, the CW normalization option is enabled in FDTD simulations, and it has also been used for all the simulation cases to get the response of the system in frequency domain. This helps to obtain the reflection, transmission, and absorption of a device.

The CW-generation script is added to measure the total absorbed power vs frequency and the short circuit current density (Jsc).

CHAPTER FOUR

RESULTS AND DISCUSSION

This chapter will present and analyse simulated findings for the optical study of three different types of device geometry (planar, axial micropillar, and radial micropillar) with variations in some of their physical dimensions (height, diameter, and pitch).

4.0 Introduction

According to computational analysis, micropillar ZnO/ZnTe solar cells typically have a higher degree of light absorption and a lower quantity of light reflection. The mathematical expressions for how absorption relate to reflection and transmission is;

$$A = 1 - R - T \quad (1)$$

Where A is absorption, R is reflection and T is transmission.

Therefore, absorption is based on a device's relative transmission and reflection levels.

4.1 Geometrical Effects

This section explores the impact of various device geometries in order to distinguish between micropillars and planar ZnO/ZnTe solar cells with greater optical performance. To accomplish this, the planar solar cell device's height as well as the heights of the two suggested micropillar solar cell devices have both been set at 1.5 μm. The various geometries / structures considered for this simulation are planar (marked in black), axial (marked in red), and radial (marked in blue). Their simulation outcomes for transmission, reflection and absorption are represented graphically in Figure 4.1 ~ Figure 4.6.

Transmission profile of geometries

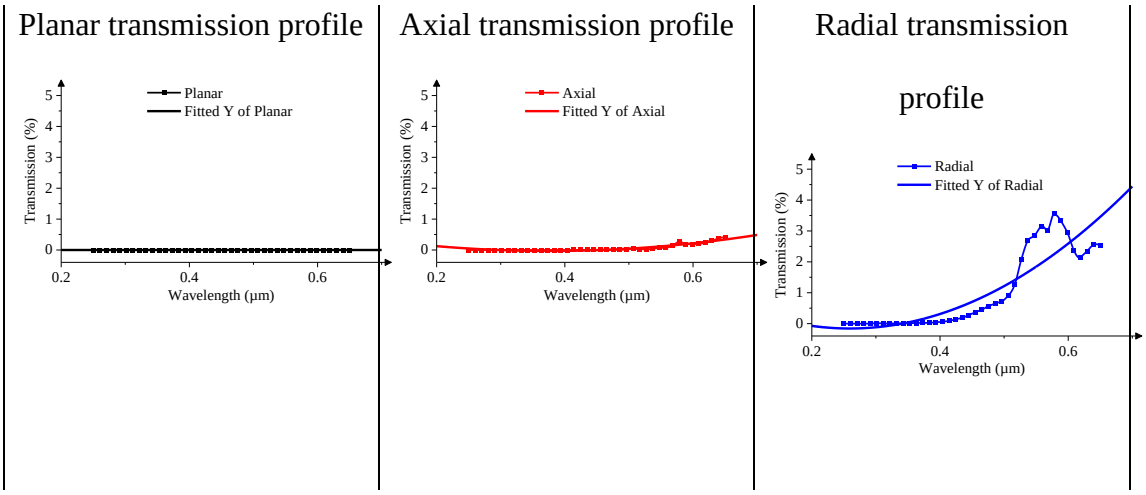

Figure 0.1: Light transmission profiles in planar, axial and radial ZnO/ZnTe Micropillar solar cell structures.

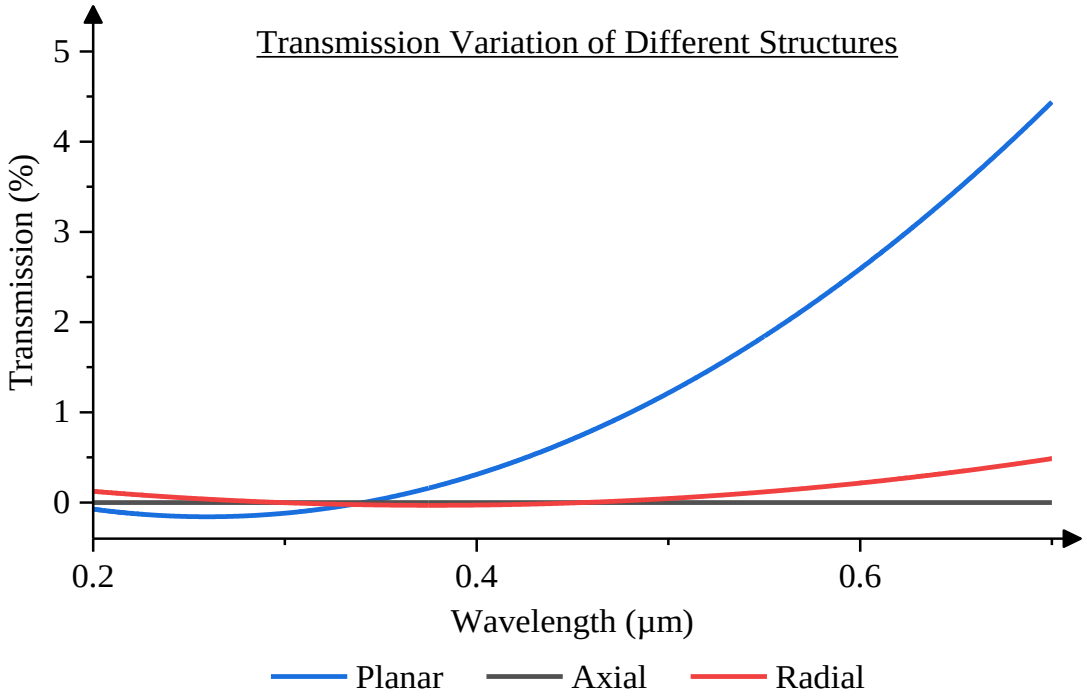

Figure 0.2: Comparative graph of light transmission percentage of three different structures of ZnO/ZnTe solar cells.

Reflection profile of geometries

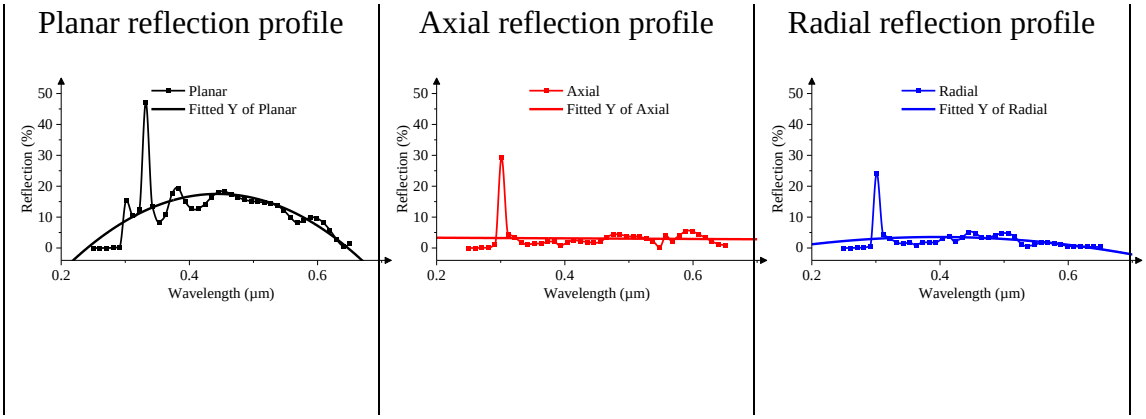

Figure 0.3: Light reflection profiles in planar, axial and radial ZnO/ZnTe micropillar solar cell structures.

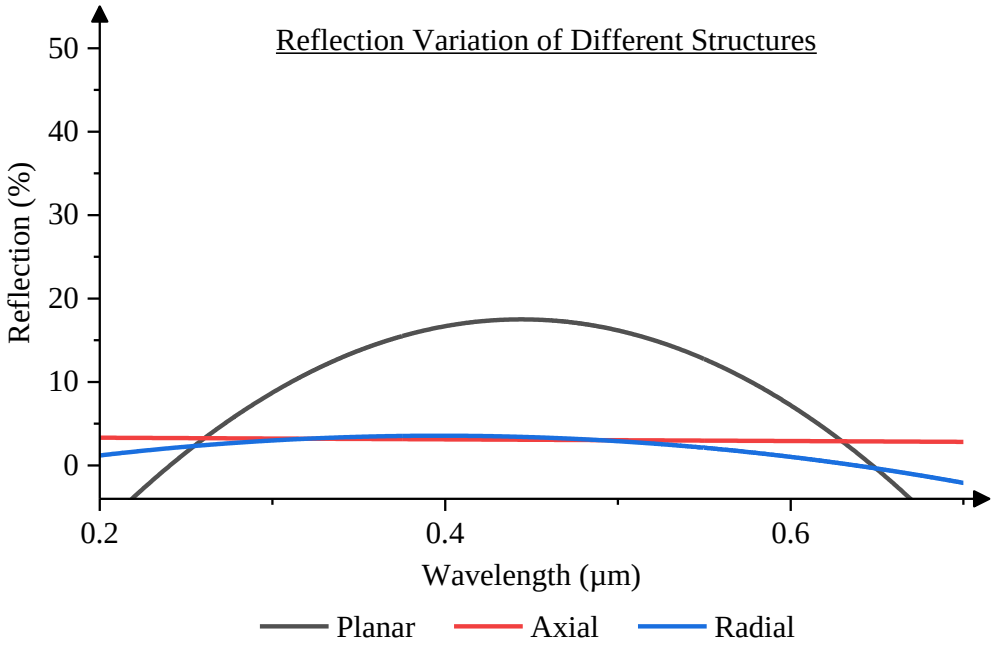

Figure 0.4: Comparative graph of light reflection percentage of three different structures of ZnO/ZnTe solar cells.

Absorption profile of geometries

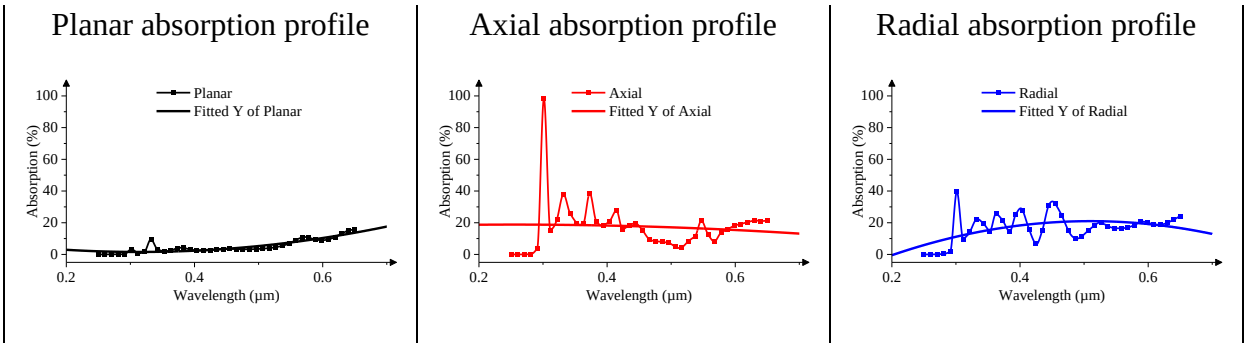

Figure 0.5: Light absorption profiles in planar, axial and radial ZnO/ZnTe micropillar solar cell structures.

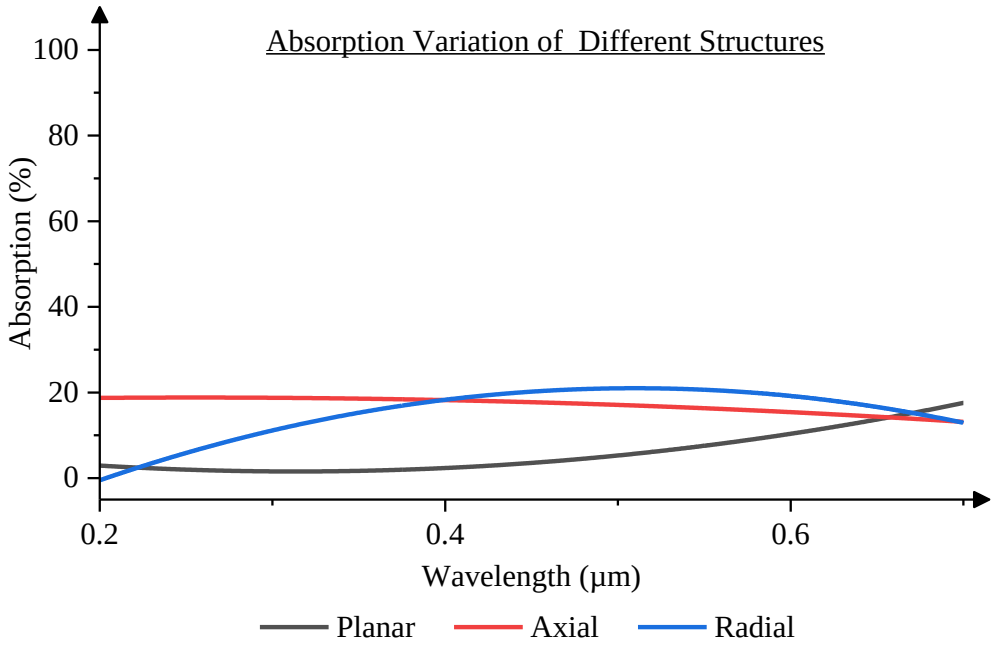

Figure 0.6: Comparative graph of light absorption percentage of three different structures of ZnO/ZnTe solar cells.

Different Structure Devices Analysis

The results in Figure 4.2 show that the planar solar cell device allows for fewer light transmission, although with an increasing trend. Whereas the suggested micropillar solar cell devices performed better at wavelengths below 0.6 µm and with a declining trend.

Contrary to transmission, Figure 4.4 shows that radial (core-shell) ZnO/ZnTe micropillar solar cell has the lowest reflection relative to all the others across the entire wavelength (0.25 μm ~ 0.65 μm) range under consideration. As a result, the use of micropillars in the device construction reduces light reflection. Figure 4.6 graph demonstrates that the two suggested micropillar devices have an absorption difference that is twenty five percent (25%) larger than that of the planar solar cell device of the same material. Axial ZnO/ZnTe micropillar solar cells exhibit the highest average absorption for wavelengths below 0.4 μm, but radial (core-shell) micropillar solar cells exhibit superior absorption for wavelengths above 0.4 μm. In conclusion, the pillar-based design outperforms the traditional planar solar cell in terms of performance.

4.2 Pillar Height Effect

In micropillar devices, the height of the pillar has a significant impact on how much light is absorbed, transmitted, and reflected. This effect has been the subject of several theoretical and experimental studies (Liao & Yi, 2009). In order to absorb all the incident light, a system must adhere to the equation (2) below:

$$H > 1/\alpha \tag{2}$$

where H = length of the pillar / thickness of the absorber layer, $1/\alpha$ = optical length

This equation suggests that in order for the system to completely absorb the incident light, its thickness must be greater than the light's optical length (Sellai, 2013). As a result, the influence of height on the light interaction of ZnO/ZnTe micropillar solar cells will be examined in this section. The ZnO/ZnTe micropillar solar cell device's pitch and diameter will remain constant at 0.5 μm and 200 nm, while altering only the pillar height. This is done to modify the pillar height and enhance the efficiency of a pillar-based solar cell.

4.2.1 Effect of Axial Absorber Pillar Height Variation

In this simulation, the emitter (ZnO height = 0.5 µm) component was kept constant while the absorber (ZnTe) component of the pillar was varied between 0.8 µm and 1.2 µm. The absorber heights considered for this simulation are 0.8 µm (marked in black), 1.0 µm (marked in red) and 1.2 µm (marked in blue). Their simulation outcomes for transmission, reflection and absorption are represented graphically in Figures 4.7 ~ Figure 4.12.

Transmission profile of different axial absorber heights

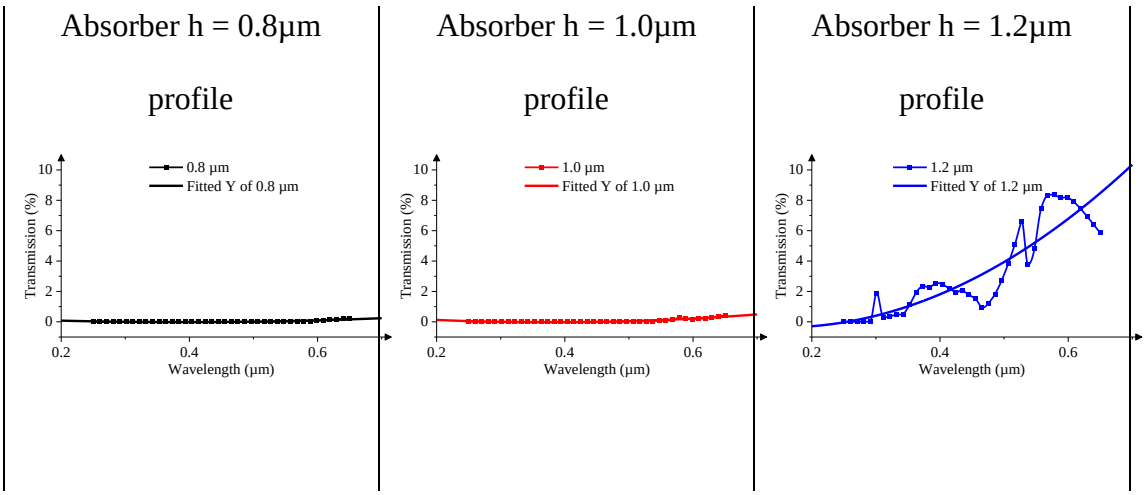

Figure 0.7: Light transmission profiles of different axial absorber heights in the range of 0.8µm to 1.2µm for a ZnO/ZnTe micropillar solar cell pillars.

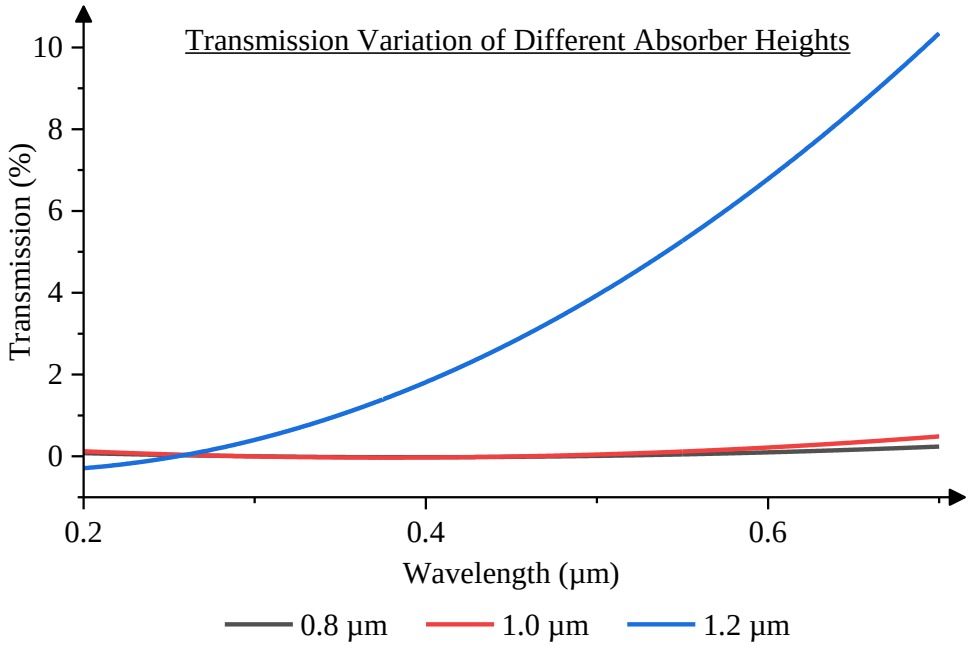

Figure 0.8: Comparative graph of light transmission percentage of three different axial absorber heights of ZnO/ZnTe micropillar solar cells.

Reflection profile of different axial absorber heights

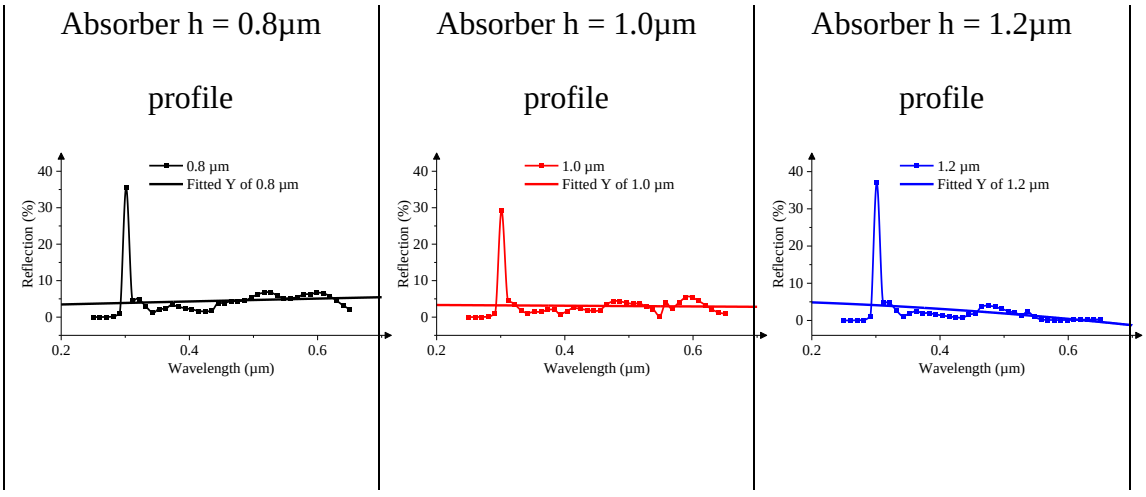

Figure 0.9: Light reflection profiles of different axial absorber heights in the range of 0.8µm to 1.2µm for a ZnO/ZnTe micropillar solar cell pillars.

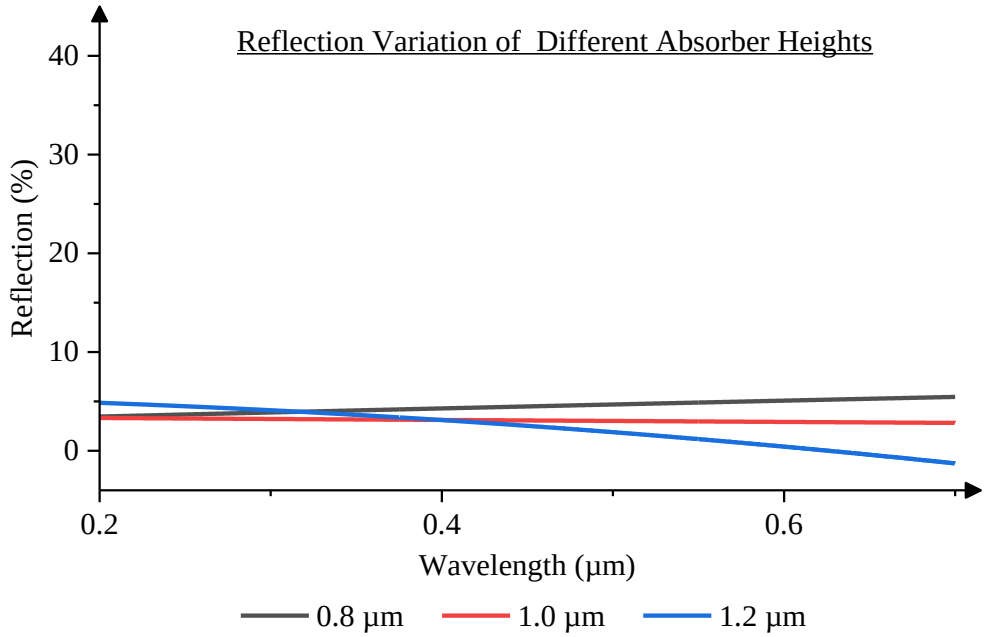

Figure 0.10: Comparative graph of light transmission percentage of three different axial absorber heights of ZnO/ZnTe micropillar solar cells.

Absorption profile of different axial absorber heights

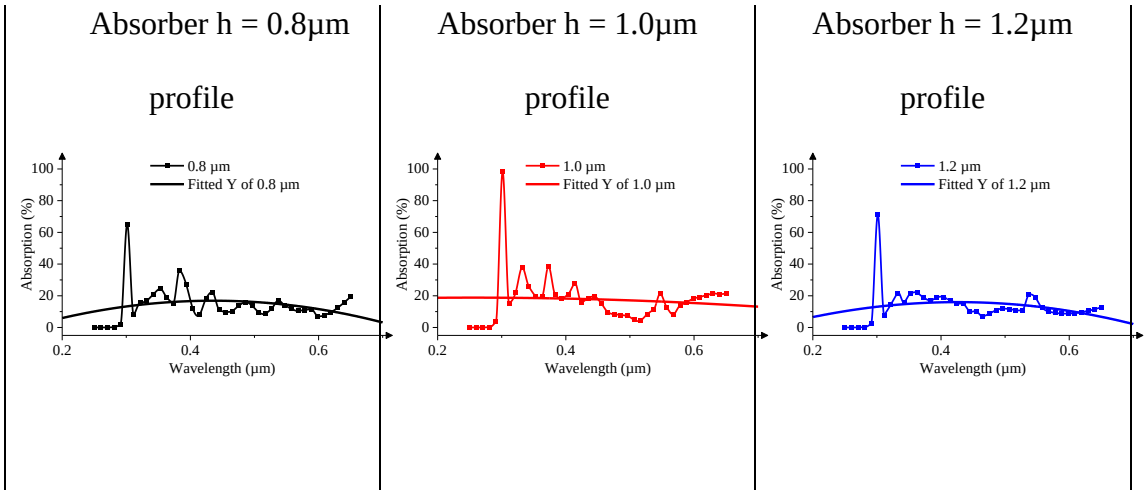

Figure 0.11: Light reflection profiles of different axial absorber heights in the range of 0.8µm to 1.2µm for a ZnO/ZnTe micropillar solar cell pillars.

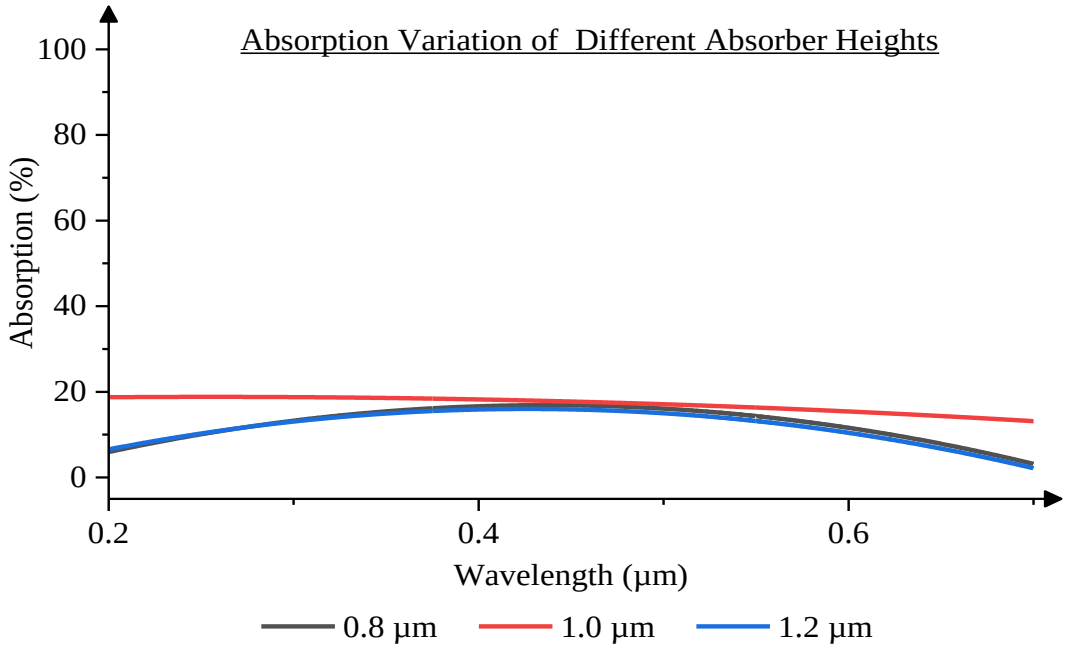

Figure 0.12: Comparative graph of light absorption percentage of three different axial absorber heights of ZnO/ZnTe micropillar solar cells.

Axial Absorber Pillar Height Variation Analysis

The data in Figure 4.8 demonstrate a pattern that transmission increases with decreasing pillar height for wavelengths below 0.3 µm, while also shows the reverse trend for wavelengths above 0.3 µm, where transmission increases with rising pillar height. Light is more effectively absorbed at 1.0 µm height, which is depicted in Figure 4.8., Figure 4.10 and Figure 4.12 by the red colour due to moderate reflection and transmission. Otherwise, Figure 4.12 shows that a drop in pillar height increases light absorption, Figure 4.8 shows a decrease in transmission, and Figure 4.10 shows a slight rise in reflection. But according to earlier experimental results, efficiency sharply enhanced when longer nanopillar arrays of CdS were incorporated into a polycrystalline CdTe thin film (Fan et al., 2009).

4.2.2 Effect of Axial Emitter Pillar Height

This section varies the height of the emitter (ZnO) component of the micropillar between 0.3 µm ~ 0.7 µm while maintaining the height of the absorber (ZnTe) component at 1.0 µm. The emitter heights considered for this simulation are 0.3 µm (marked in black), 0.5 µm (marked in red) and 0.7 µm (marked in blue). The transmission, reflection and absorption outcomes of their simulation are represented graphically in Figure 4.13 ~ Figure 4.18.

Transmission profiles of different axial emitter heights

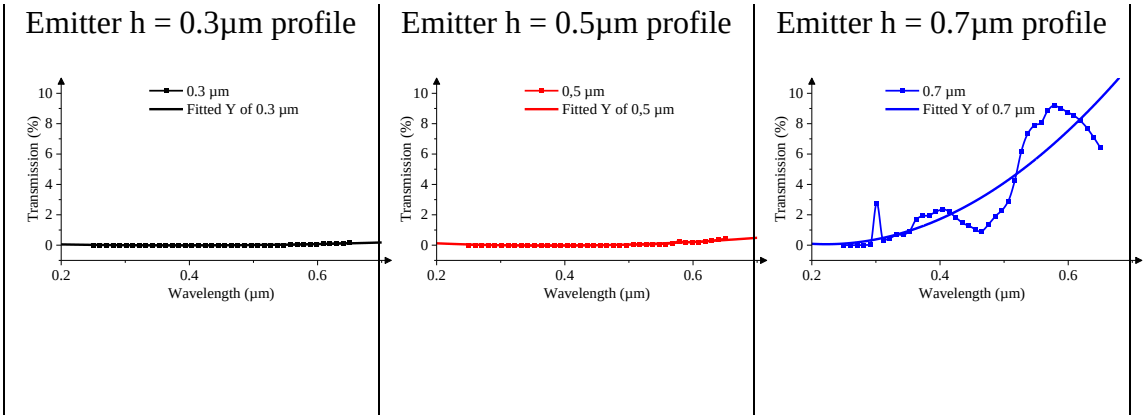

Figure 0.13: Light transmission profiles of different axial emitter heights in the range of 0.3µm to 0.7µm for a ZnO/ZnTe micropillar solar cell pillars.

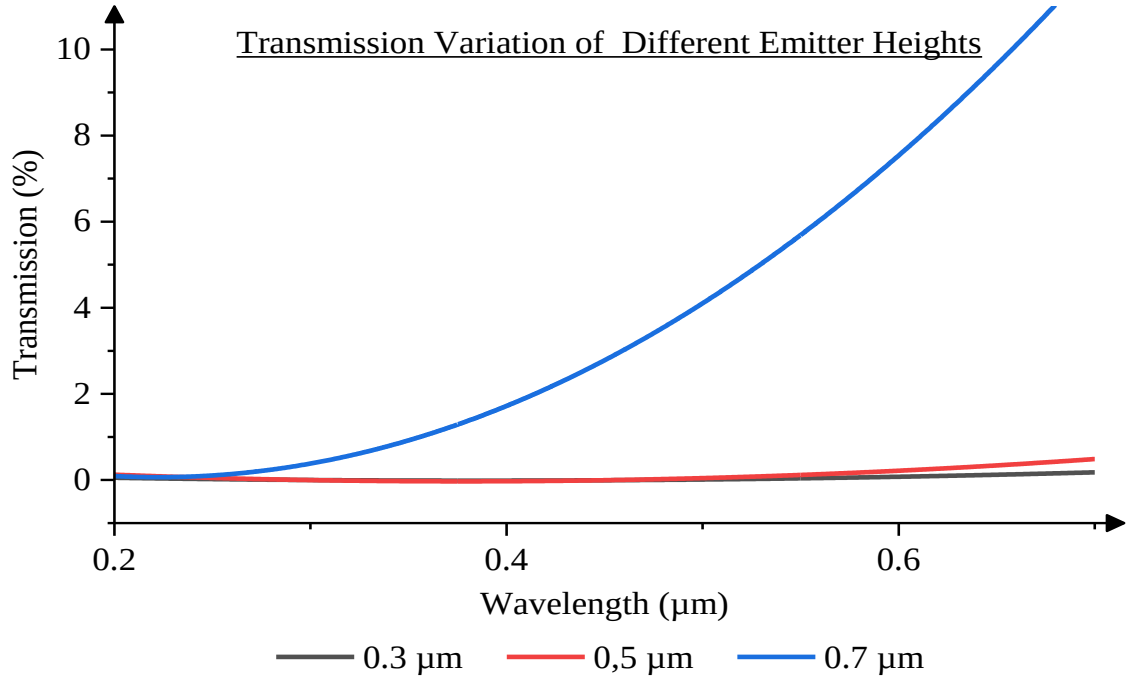

Figure 0.14: Comparative graph of light transmission percentage of three different axial emitter heights of ZnO/ZnTe micropillar solar cells.

Reflection profiles of different axial emitter heights

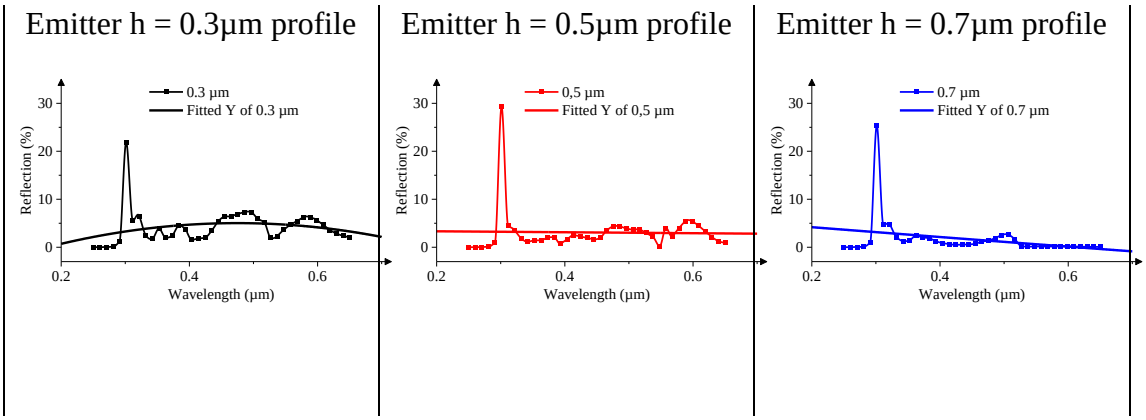

Figure 0.15: Light reflection profiles of different axial emitter heights in the range of 0.3µm to 0.7µm for a ZnO/ZnTe micropillar solar cell pillars.

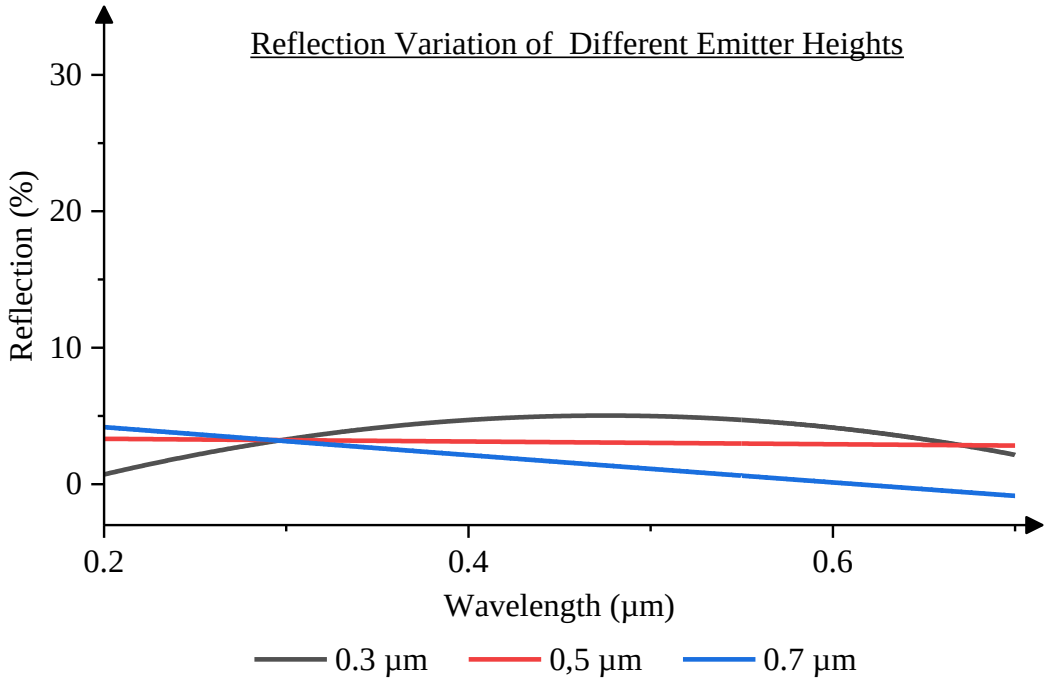

Figure 0.16: Comparative graph of light reflection percentage of three different axial emitter heights of ZnO/ZnTe micropillar solar cells.

Absorption profiles of different axial emitter heights

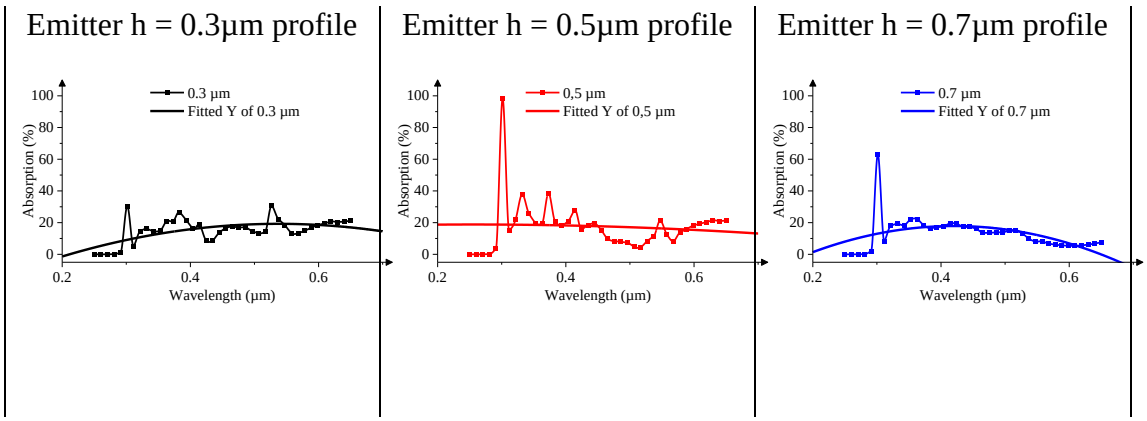

Figure 0.17: Light absorption profiles of different axial emitter heights in the range of 0.3µm to 0.7µm for a ZnO/ZnTe micropillar solar cell pillars.

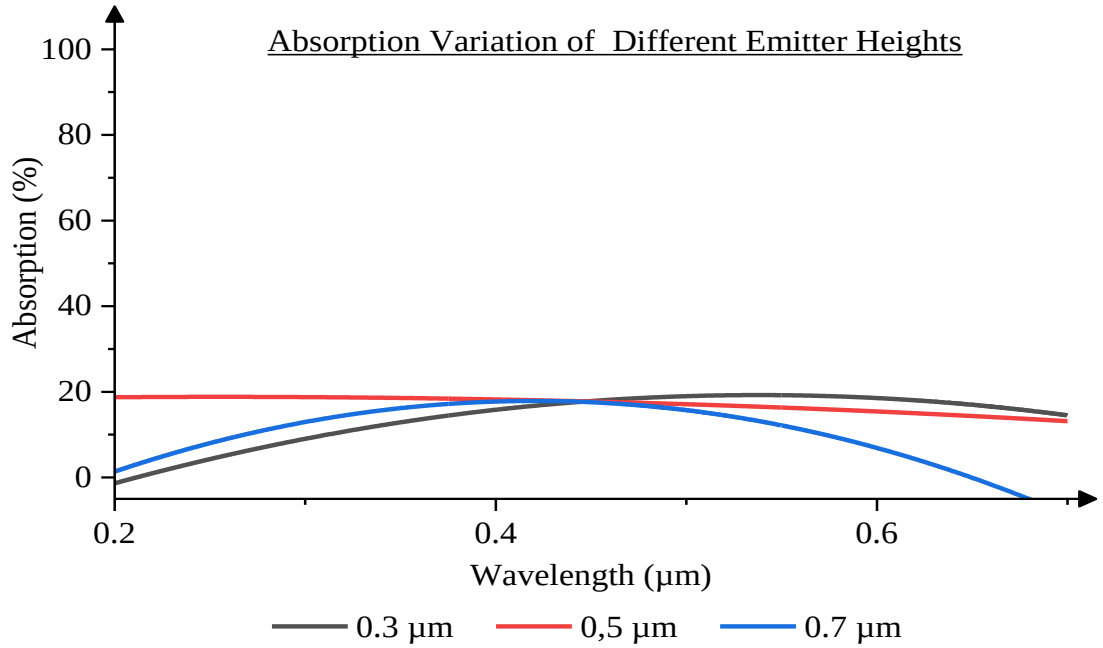

Figure 0.18: Comparative graph of light reflection percentage of three different axial emitter heights of ZnO/ZnTe micropillar solar cells.

Axial Emitter Pillar Height Variation Analysis

Figure 4.14 illustrates how increasing the height of the emitter pillar considerably increases the device's ability to transmit light within the entire wavelength range of 0.25 µm ~ 0.65 µm, while also decreasing the reflection of light for wavelengths longer than 0.3 µm as shown in Figure 4.16. Additionally, the results demonstrate that the emitter pillar height of 0.5 µm (shown in red) offers a higher light absorption rate throughout the full wavelength range (0.25 µm ~ 0.65 µm) than the other two emitter heights (0.3 µm and 0.7 µm) taken into account in Figure 4.18.

4.2.3 Effect of Radial Pillar Height

A radial (core-shell) ZnO/ZnTe solar cell device's micropillars are made up of an inner ZnO core and an outer ZnTe shell. Both the core and the shell have the same height. As a result, they will both be raised or lowered by the same value. In this simulation,

micropillar heights of 1.3 µm (marked in black), 1.5 µm (marked in red), and 1.7 µm are taken into consideration (marked in blue). The transmission, reflection and absorption findings of their simulation are shown graphically in Figure 4.19 ~ Figure 4.24.

Transmission profiles of different radial (core-shell) pillar heights

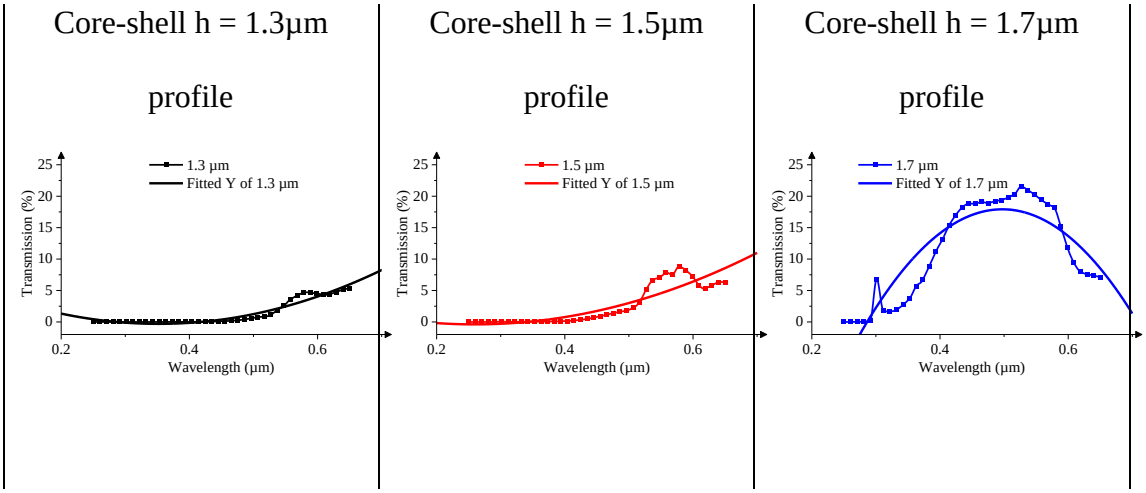

Figure 0.19: Light transmission profiles of different radial (core-shell) pillar heights in the range of 1.3µm to 1.7µm for a ZnO/ZnTe micropillar solar cell.

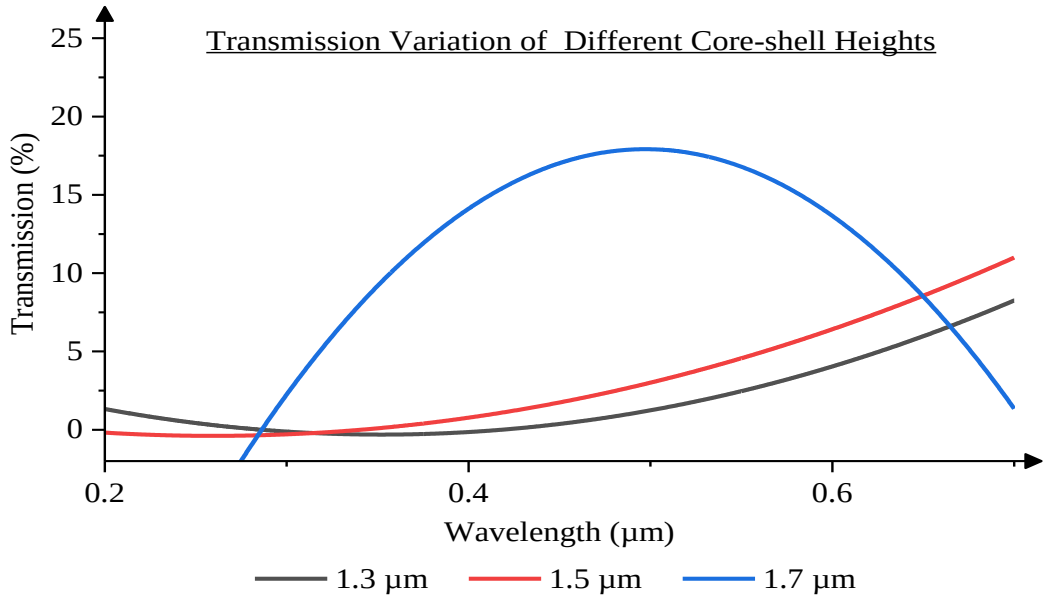

Figure 0.20: Comparative graph of light transmission percentage of three different radial (core-shell) pillar heights of ZnO/ZnTe micropillar solar cells.

Reflection profiles of different radial (core-shell) pillar heights

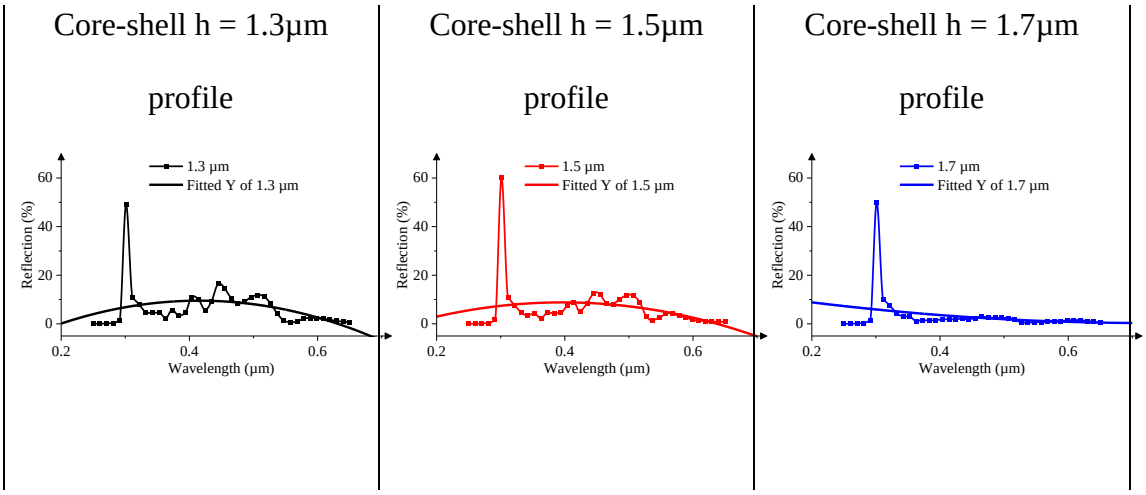

Figure 0.21: Light reflection profiles of different radial (core-shell) pillar heights in the range of 1.3µm to 1.7µm for a ZnO/ZnTe micropillar solar cell.

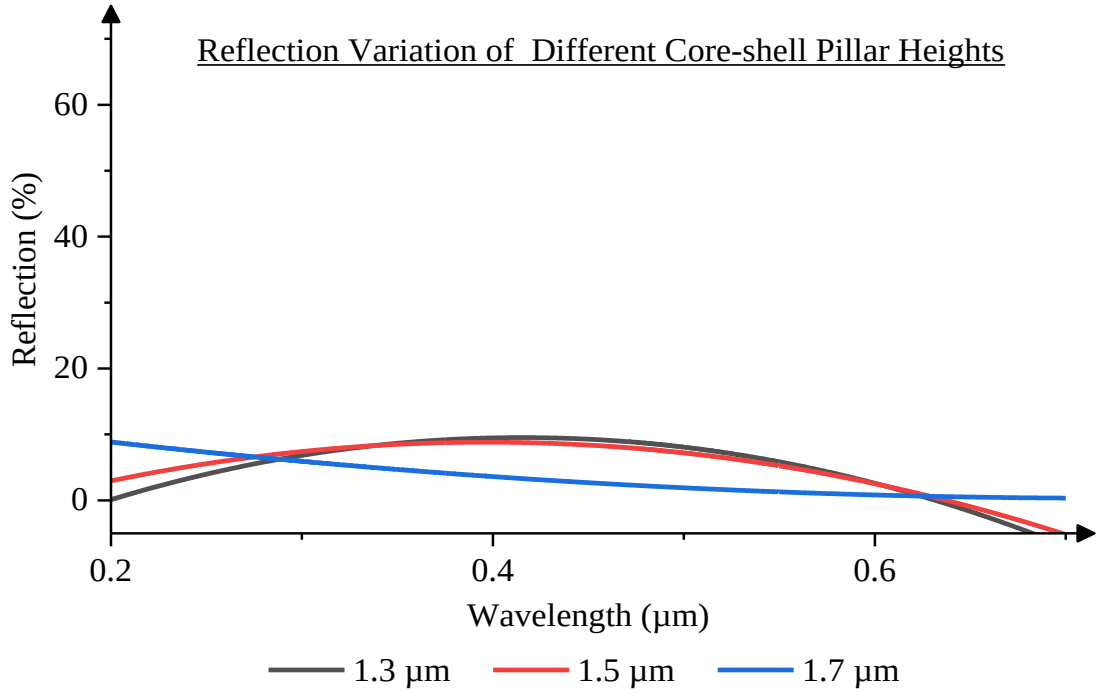

Figure 0.22: Comparative graph of light reflection percentage of three different radial (core-shell) pillar heights of ZnO/ZnTe micropillar solar cells.

Absorption profiles of different radial (core-shell) pillar heights

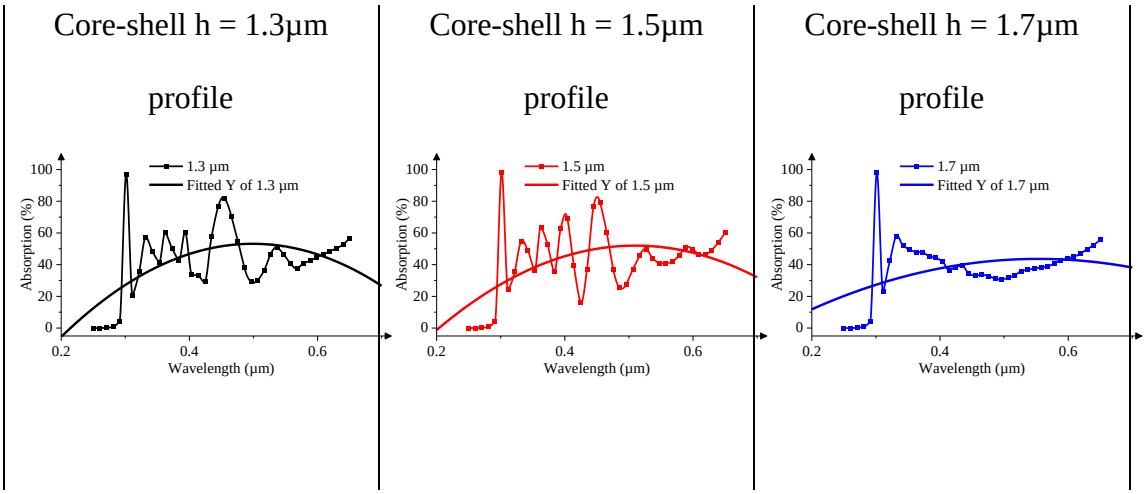

Figure 0.23: Light absorption profiles of different radial (core-shell) pillar heights in the range of 1.3µm to 1.7µm for a ZnO/ZnTe micropillar solar cell.

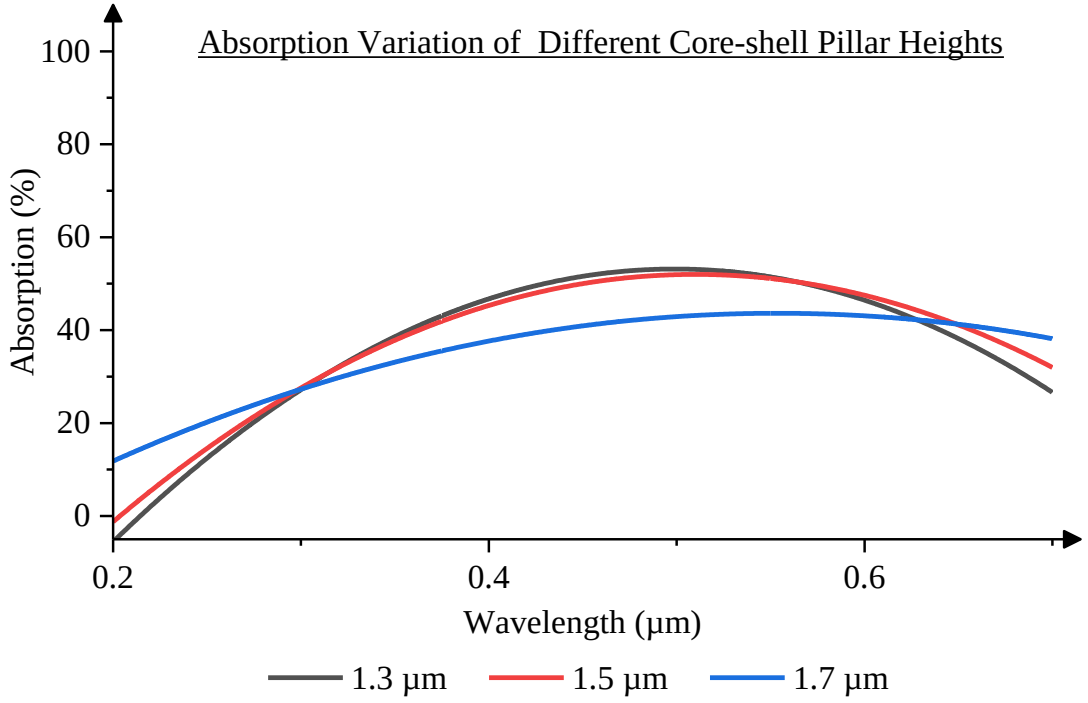

Figure 0.24: Comparative graph of light absorption percentage of three different radial (core-shell) pillar heights of ZnO/ZnTe micropillar solar cells.

Radial Pillar Height Variation Analysis

The analysis's consideration of pillar heights between 1.3 μm to 1.7 μm reveals an increase in light transmission when the height of radial (core-shell) pillars is raised between wavelengths of 0.3 μm and 0.625 μm, as illustrated in Figure 4.20. The graph of light reflection in Figure 4.22 likewise depicts a range that significantly decreases as the pillar height increases. Figure 4.24 demonstrates that for wavelengths between 0.3 μm and 0.625 μm, increasing the height of the pillar only results in a decrease in the absorption of radiant energy, and vice versa for other wavelengths.

4.3 Pillar Diameter Effect

Another crucial factor that influences the solar cell's performance is the pillar diameter. This section investigates the influence of micropillar diameter on the optical performance of an axial and radial (core-shell) ZnO/ZnTe solar cell system. The influence of different micropillar diameter values was studied. During the pillar diameter / thickness research, the pillar height and pitch were held constant at 1.5 μm and 0.5 μm, respectively. The single influence of the diameter may be properly observed by holding these two factors constant at certain levels.

4.3.1 Effect of Axial Micropillar Diameter

An axial ZnO/ZnTe solar cell device's micropillars are made up of a p-ZnTe absorber at the bottom and a ZnO emitter on top. They both share the same pillar diameter. Therefore, their pillar diameter will be raised or lowered by the same value in this part. For this simulation, pillar diameters of 160 nm (shown in black), 200 nm (shown in red), and 240 nm were taken into consideration (marked in blue). The transmission, reflection and absorption outcomes of their simulation are represented graphically in Figure 4.25 ~ Figure 4.30.

Transmission profiles of different axial pillar diameters / thickness

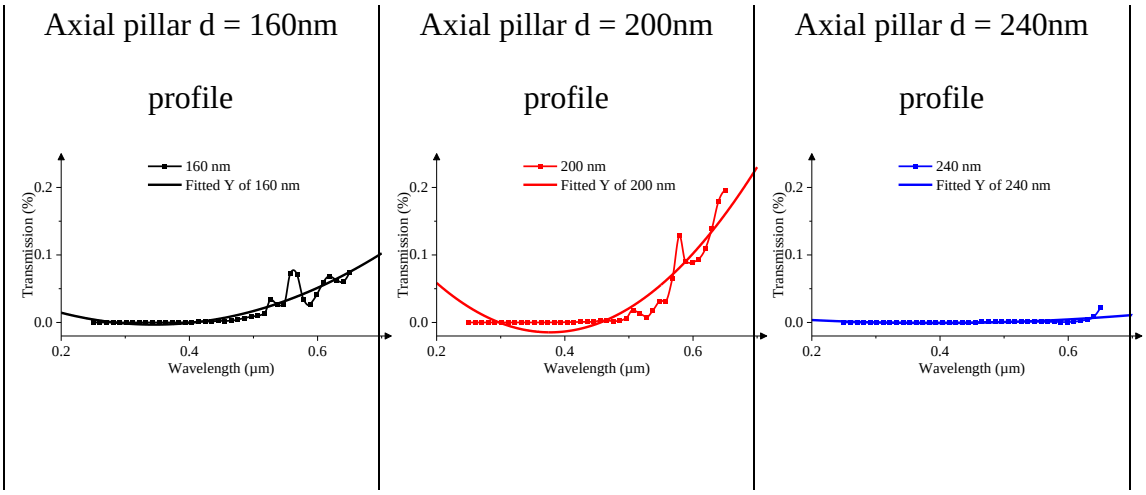

Figure 0.25: Light Transmission profiles of different axial pillar diameter / thickness in the range of 160nm to 240nm for a ZnO/ZnTe micropillar solar cell.

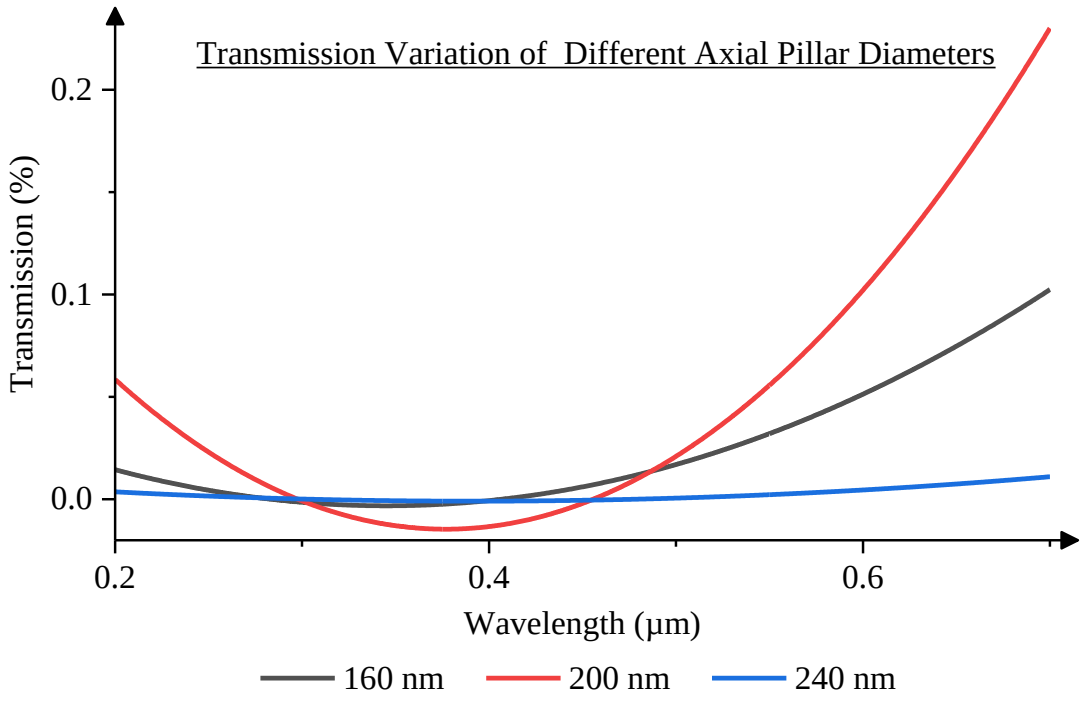

Figure 0.26: Comparative graph of light transmission percentage of three different axial pillar diameter of ZnO/ZnTe micropillar solar cells.

Reflection profiles of different axial pillar diameters / thickness

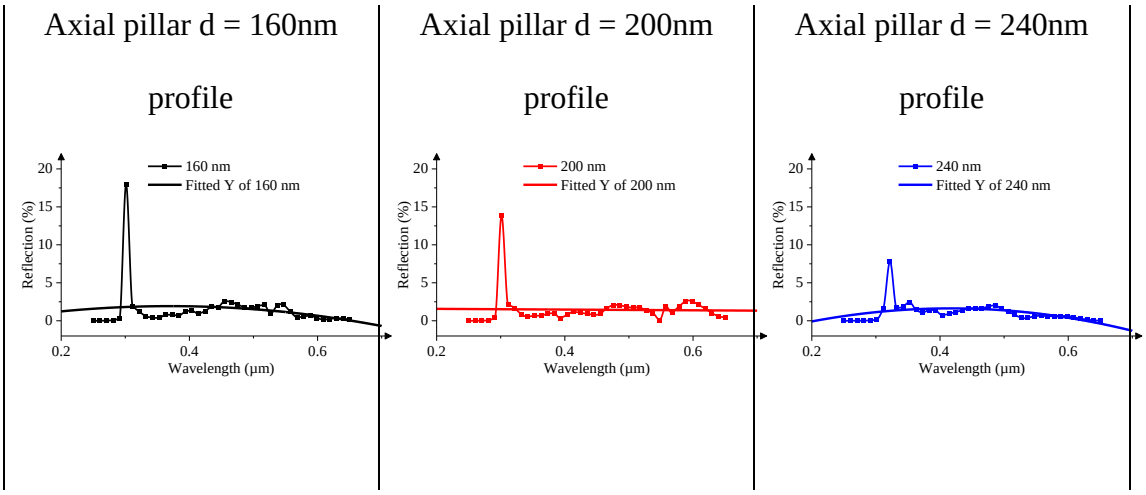

Figure 0.27: Light reflection profiles of different axial pillar diameter / thickness in the range of 160nm to 240nm for a ZnO/ZnTe micropillar solar cell.

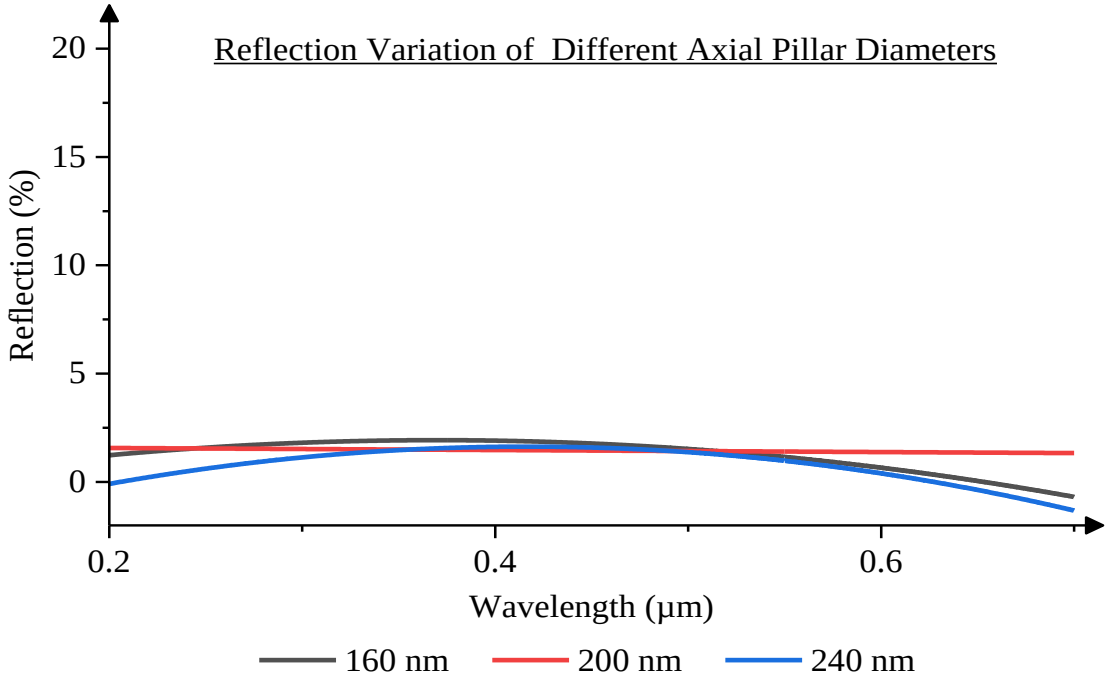

Figure 0.28: Comparative graph of light transmission percentage of three different axial pillar diameter of ZnO/ZnTe micropillar solar cells.

Absorption profiles of different axial pillar diameters / thickness

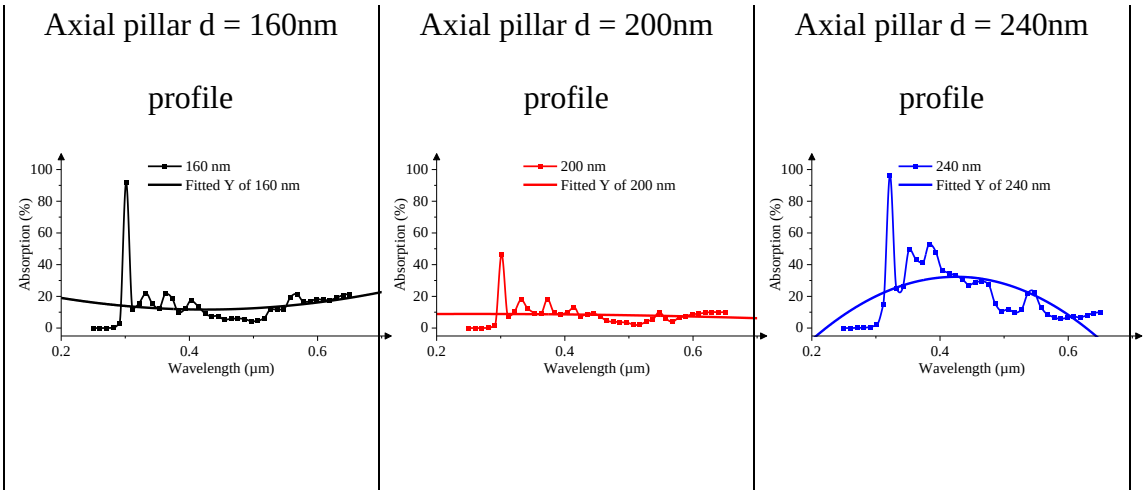

Figure 0.29: Light absorption profiles of different axial pillar diameter / thickness in the range of 160nm to 240nm for a ZnO/ZnTe micropillar solar cell.

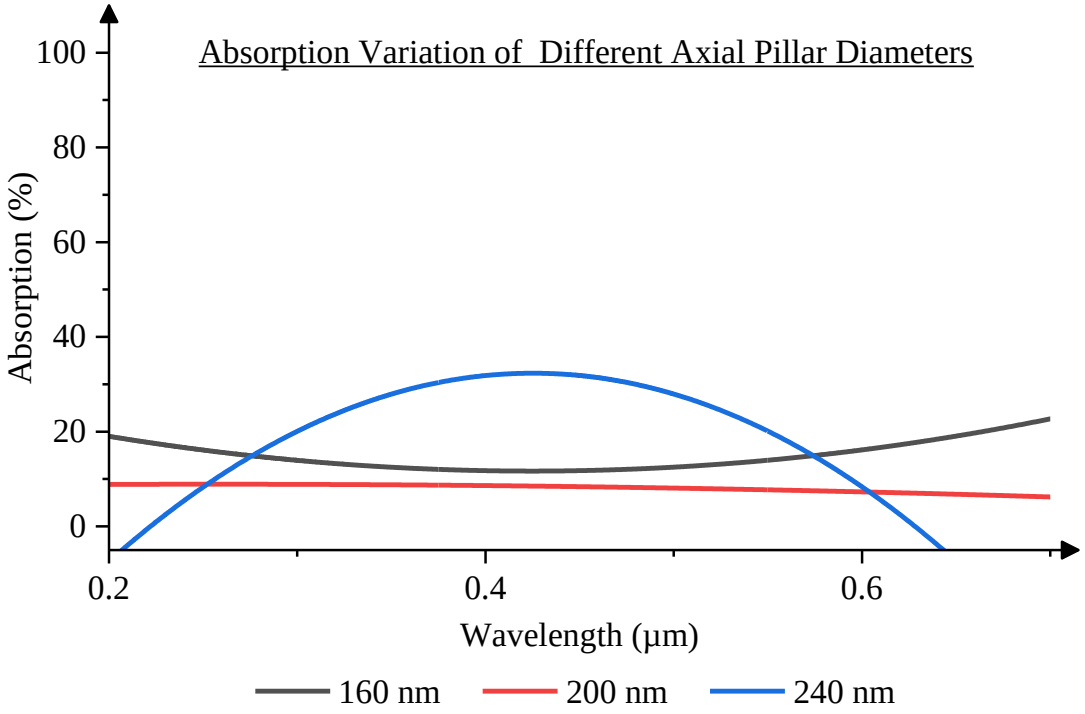

Figure 0.30: Comparative graph of light absorption percentage of three different axial pillar diameter of ZnO/ZnTe micropillar solar cells.

Axial Pillar Diameter Variation Analysis

The optical study of the ZnO/ZnTe micropillar solar cell device predicts lesser reflection of below twenty percent (20%) and a larger absorption of over twenty percent (20%) over the wavelength domain of 0.25 μm ~ 0.65 μm while adjusting the thickness of the pillars, as shown in Figure 4.28 and Figure 4.30. However, when the diameter or thickness was 240 nm, the highest absorption took place in the wavelength range of 0.3 μm ~ 0.5 μm (blue curve). Figure 4.26 shows that a pillar with a maximum diameter / thickness of 240 nm allows for the least amount of light transmission (less than 2%), whereas Figure 4.28 shows that a pillar with a diameter / thickness of 160 nm reflects the most light.

4.3.2 Effect of Radial Core Diameter

The micropillars of a radial (core-shell) ZnO/ZnTe solar cell device are composed of an inner core of ZnO and an outer shell of ZnTe. To adjust the overall diameter or thickness of the pillar, only the inner core's diameter / thickness is changed; the pillar's ZnTe outer shell diameter remains unchanged. For this simulation, the core diameters or thicknesses taken into account are 60 nm (shown in black), 100 nm (shown in red), and 140 nm (marked in blue). The transmission, reflection and absorption outcomes of their simulation are shown in Figure 4.31 ~ Figure 4.36.

Transmission profiles of different radial pillar core diameters

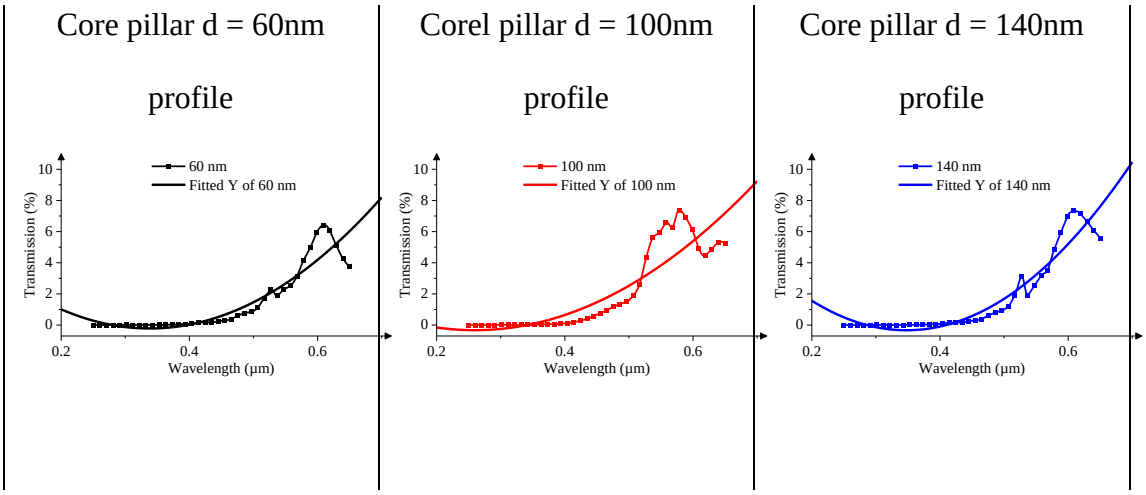

Figure 0.31: Light transmission profiles of different radial pillar core diameter in the range of 60nm to 140nm for a ZnO/ZnTe micropillar solar cell.

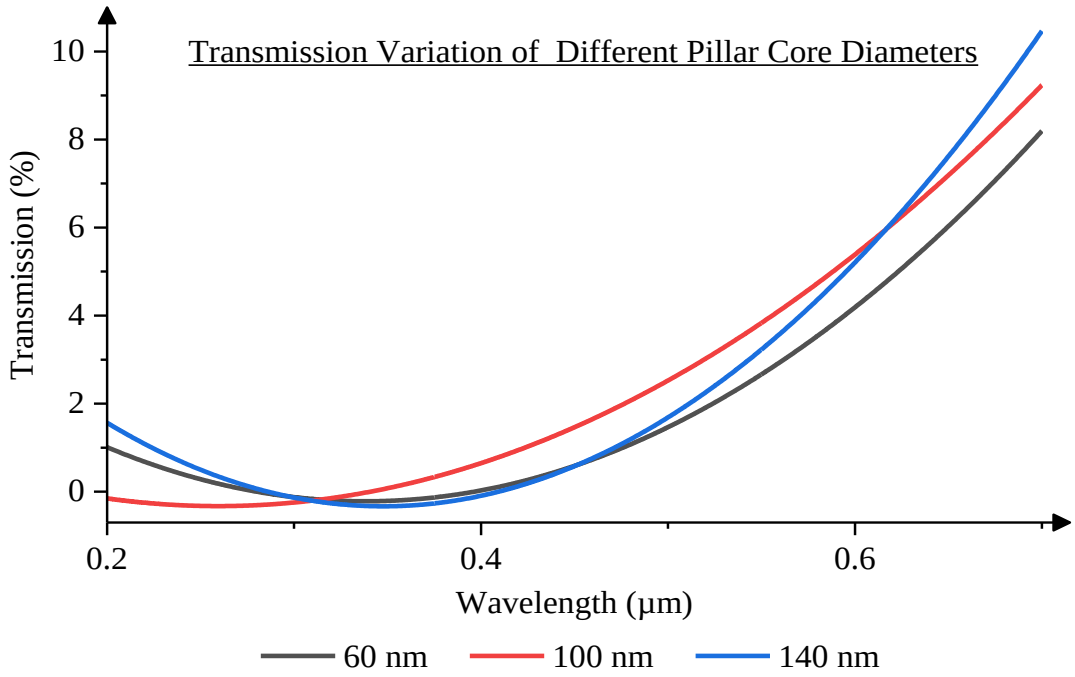

Figure 0.32: Comparative graph of light absorption percentage of three different axial pillar diameter of ZnO/ZnTe micropillar solar cells.

Reflection profiles of different radial pillar core diameters

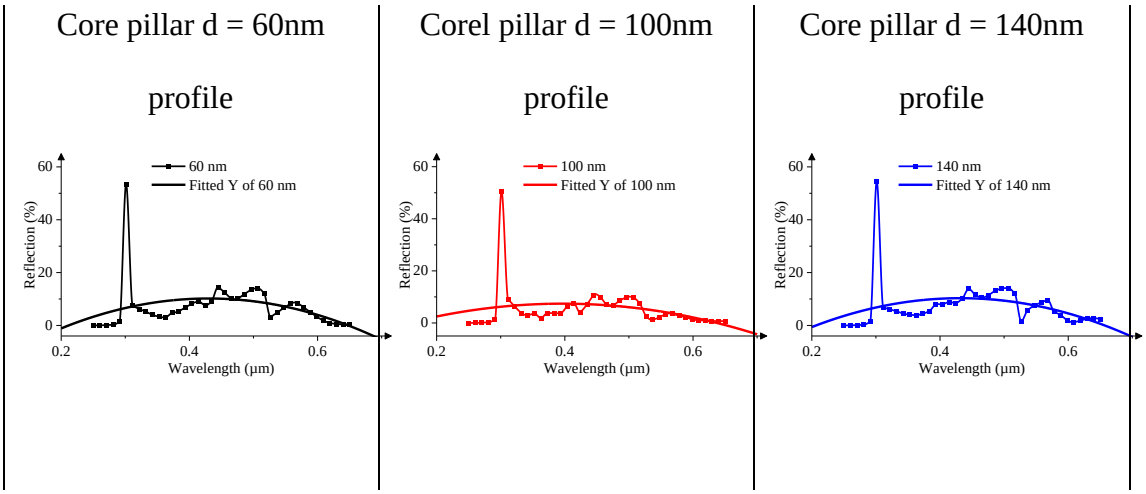

Figure 0.33: Light reflection profiles of different radial pillar core diameter in the range of 60nm to 140nm for a ZnO/ZnTe micropillar solar cell.

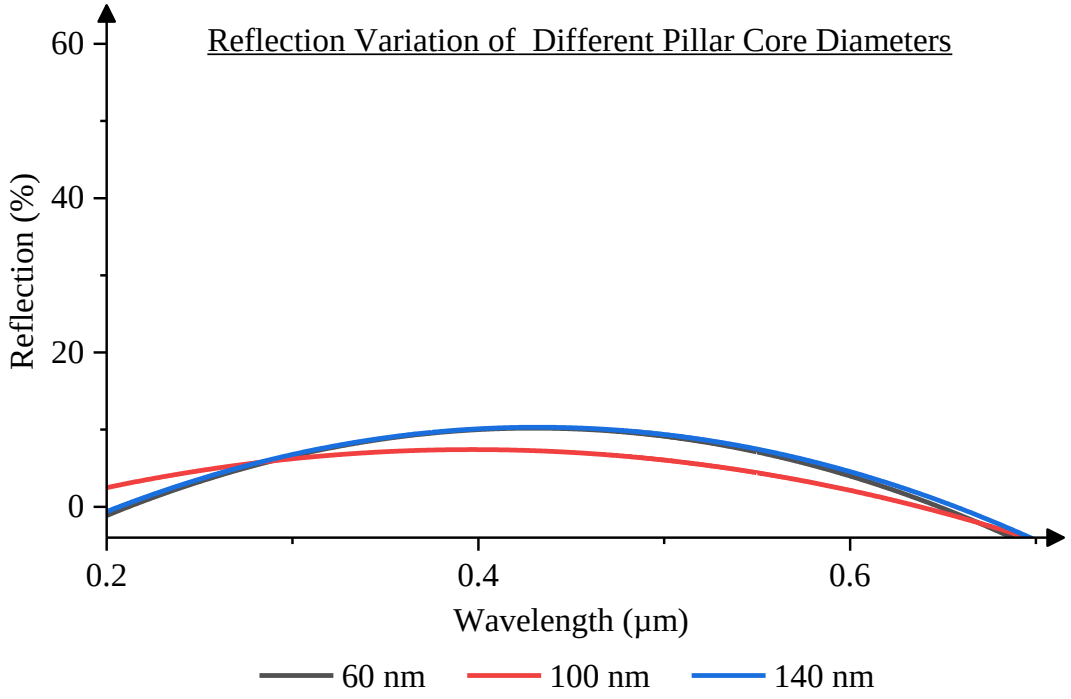

Figure 0.34: Comparative graph of light reflection percentage of three different radial pillar core diameters of ZnO/ZnTe micropillar solar cells.

Absorption profiles of different radial pillar core diameters

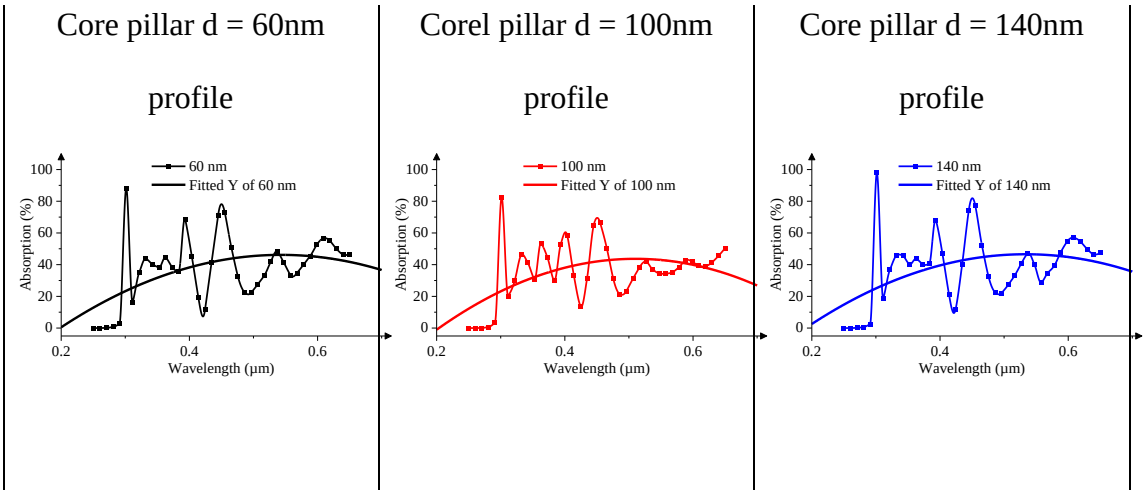

Figure 0.35: Light absorption profiles of different radial pillar core diameter in the range of 60nm to 140nm for a ZnO/ZnTe micropillar solar cell.

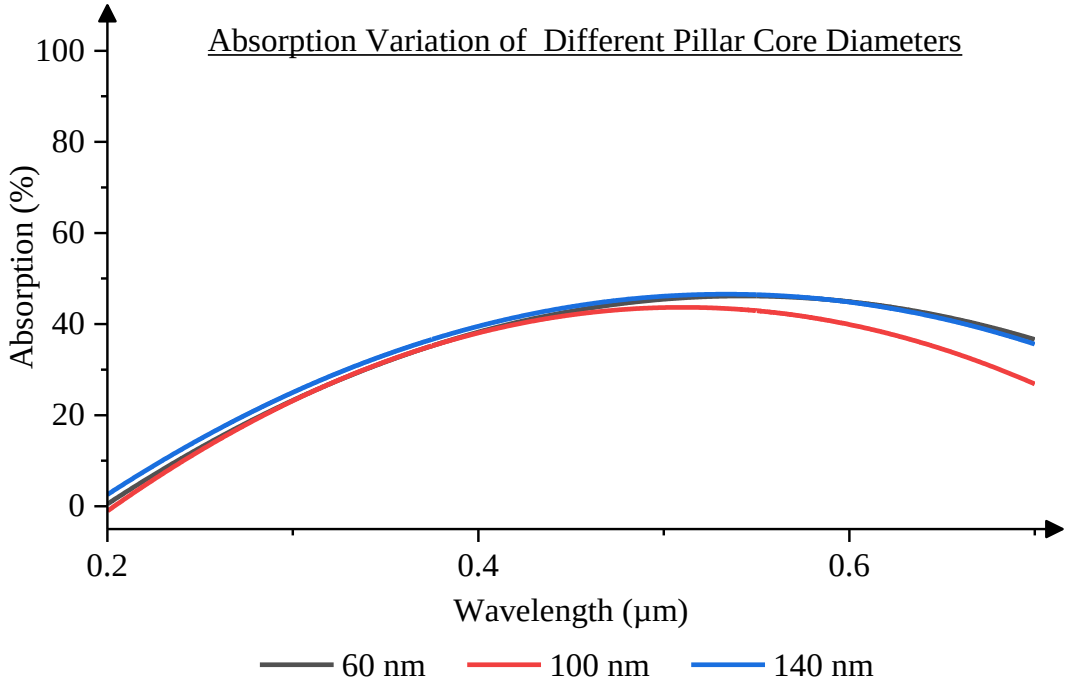

Figure 0.36: Comparative graph of light reflection percentage of three different radial pillar core diameters of ZnO/ZnTe micropillar solar cells.

Radial Core Diameter Variation Analysis

With core diameters/thickness of 60 nm and 140 nm, Figure 4.31 ~ Figure 4.36 indicates that increasing the core diameter/thickness slightly increases light transmission (in Figure 4.32), increases the light reflection (in Figure 4.34), and also increases the light absorption (in Figure 4.36) marginally. The core diameter of 100 nm rather had the lowest absorption and reflection while having a greater transmission in the 0.3 µm ~ 0.6 µm wavelength range as illustrated in Figure 4.32, Figure 4.34 and Figure 4.36.

4.3.3 Radial Shell Changing Thickness Effect

In this simulation, just the thickness of the ZnTe has been changed to modify the total diameter of the pillars. The ZnO core's diameter was held constant at 100 nm while the pillar's diameter / thickness is changed. This simulation considered outer shell thicknesses of 160 nm (indicated in black), 200 nm (marked in red), and 240 nm (marked in blue). The transmission, reflection and absorption outcomes of their simulation are represented graphically in Figure 4.37 ~ 4.42.

Transmission profiles of different radial pillar shell thickness

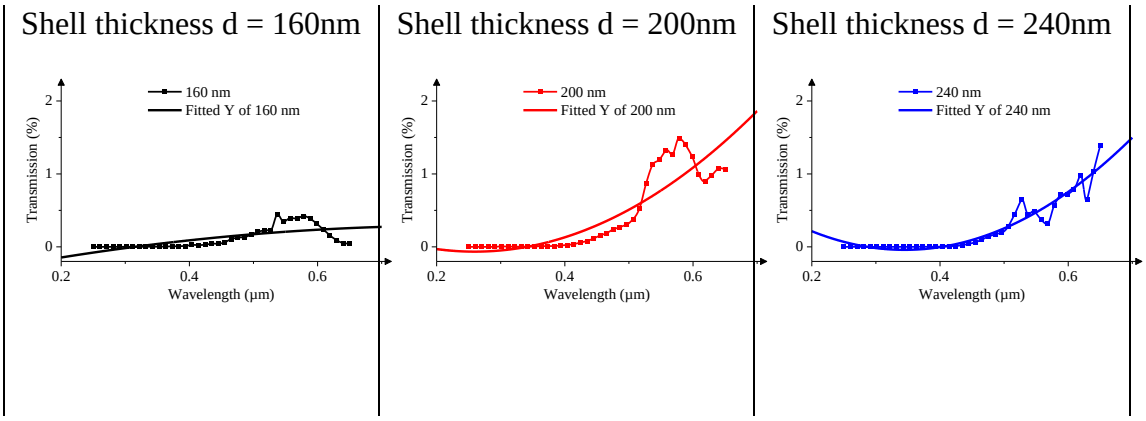

Figure 0.37: Light transmission profiles of different radial pillar shell thickness in the range of 160nm to 240nm for a ZnO/ZnTe micropillar solar cell.

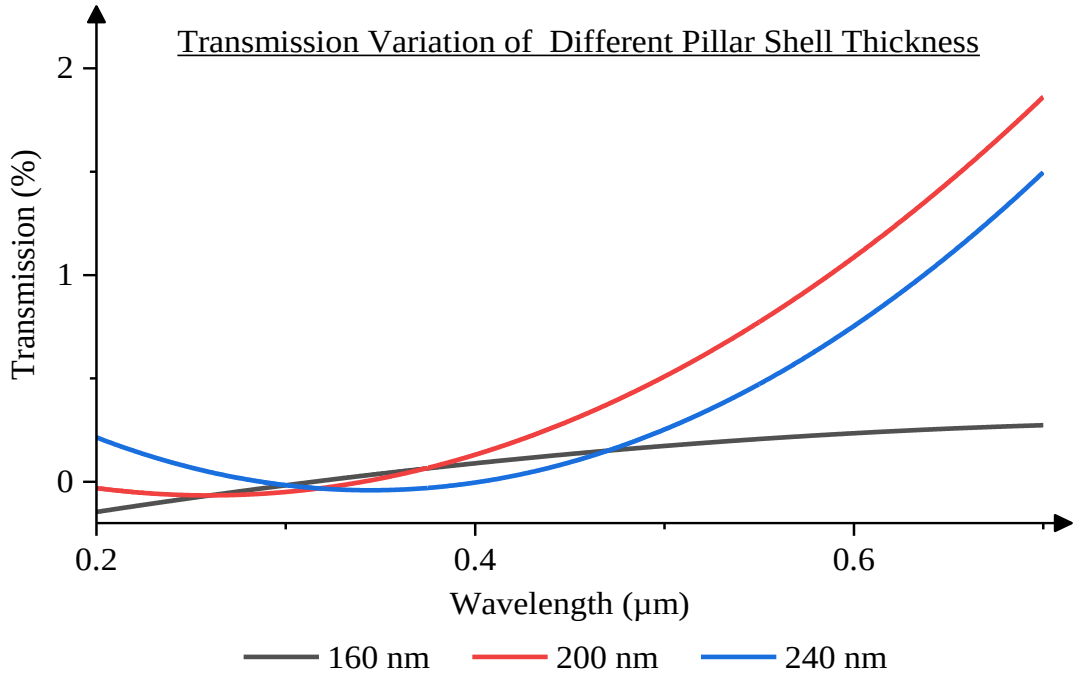

Figure 0.38: Comparative graph of light transmission percentage of three different radial pillar shell thickness of ZnO/ZnTe micropillar solar cells.

Reflection profiles of different radial pillar shell thickness

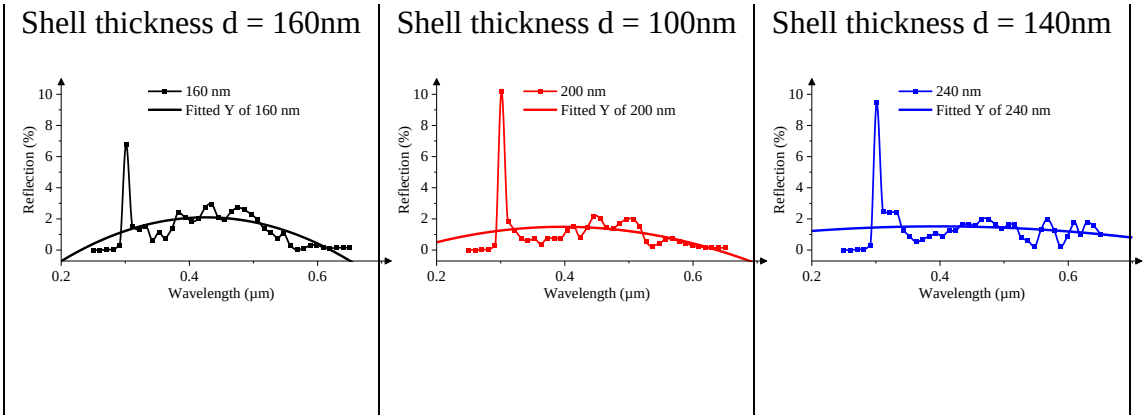

Figure 0.39: Light reflection profiles of different radial pillar shell thickness in the range of 160nm to 240nm for a ZnO/ZnTe micropillar solar cell.

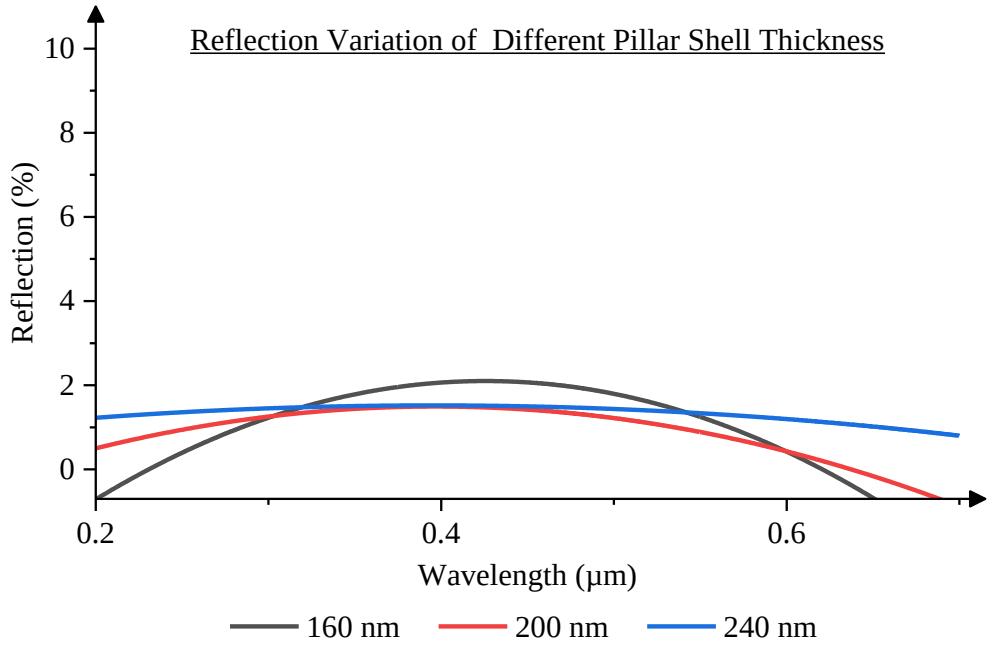

Figure 0.40: Comparative graph of light reflection percentage of three different radial pillar shell thickness of ZnO/ZnTe micropillar solar cells.

Absorption profiles of different radial pillar shell thickness

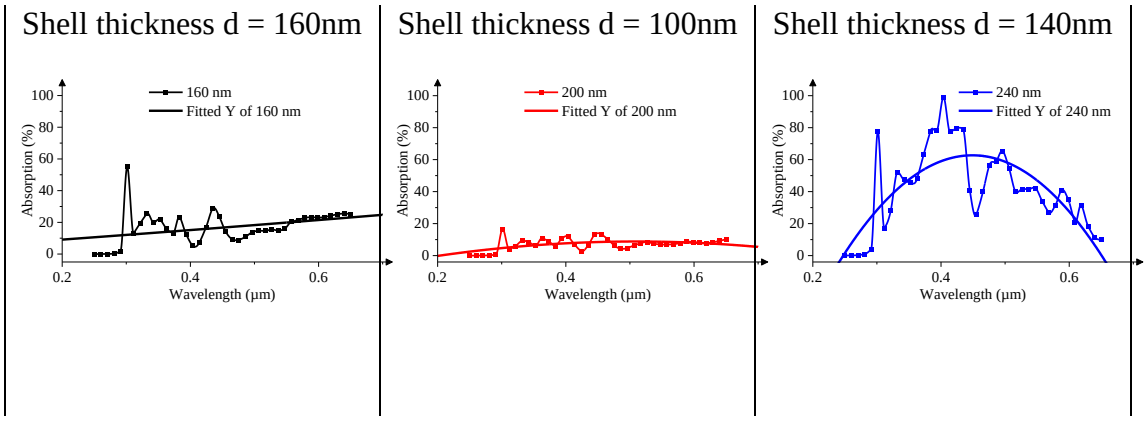

Figure 0.41: Light reflection profiles of different radial pillar shell thickness in the range of 160nm to 240nm for a ZnO/ZnTe micropillar solar cell.

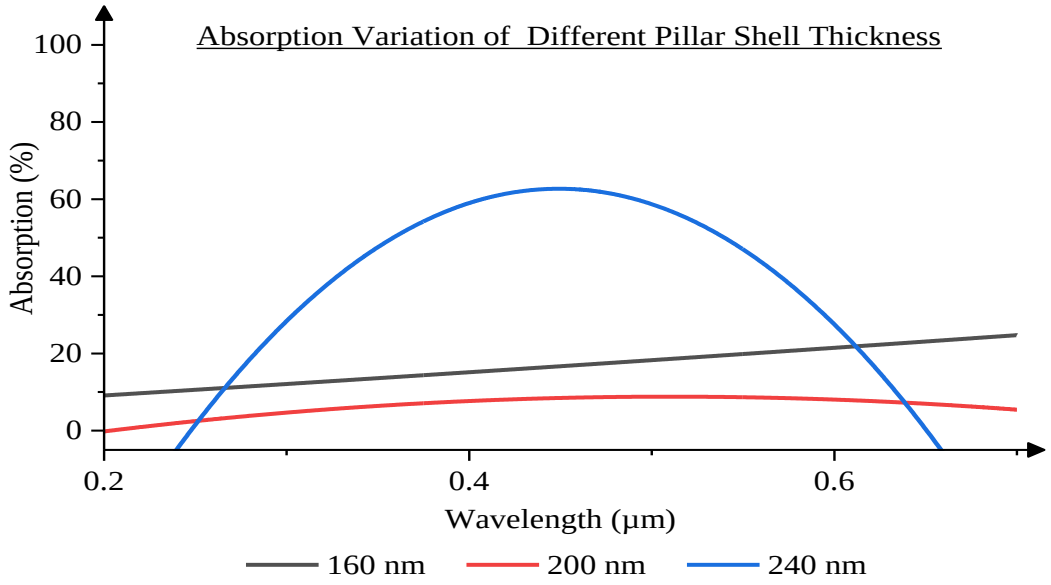

Figure 0.42: Comparative graph of light reflection percentage of three different radial pillar shell thickness of ZnO/ZnTe micropillar solar cells.

Radial Shell Thickness Variation Analysis

The result of an optical study of a micropillar solar cell made of ZnO/ZnTe in relation to the thickness of the shell (ZnTe) is depicted in Figure 4.37 ~ Figure 4.42. The reflection spectrum in Figure 4.40 illustrates how an increase in shell thickness increases the reflection, but also shows the reverse for shell thicknesses of 160 nm and 240 nm for wavelengths between 0.3 µm ~ 0.6 µm. However, the absorption spectra reveal increased absorption for the thickest shell of 240 nm in the wavelength range of 0.3 µm ~ 0.6 µm. The remainder of the visible light spectrum, however, experiences a marked reduction in light absorption.

4.4 Pillars Pitch Effect

The distance between the centres of two neighbouring pillars is referred to as the pitch parameter. Pitch variation has a big effect on how well the device performs optically. It may be utilized to determine how much light the device can absorb. The planar structure's

light trapping technique is comparable to that of two neighbouring pillars that are spaced closely together. Whereas surface recombination and material waste are more likely to occur when the distance between the pillars is greater. The ideal geometric pitch size is therefore sought. A computational effort on the effect of diameter to pitch ratio change on light trapping has been performed by (Michallon, Bucci, Morand, Zanuccoli, Consonni & Kaminski-Cachopo, 2014).

4.4.1 Axial Pillars Pitch Changing Effects

The influence of pitch between neighbouring axial pillars in the range of 0.3 µm ~ 0.7 µm is investigated in this section while other factors, such as pillar height and diameter/thickness, were held constant at 1.5 µm and 200 nm, respectively. This simulation took into account three different pitches: 0.3 µm (indicated in black), 0.5 µm (marked in red), and 0.7 µm (marked in blue). The transmission, reflection, and absorption spectra between two close pillars are shown as a function of percentage in Figure 4.43 ~ Figure 4.48.

Transmission profiles of pitch between axial pillars

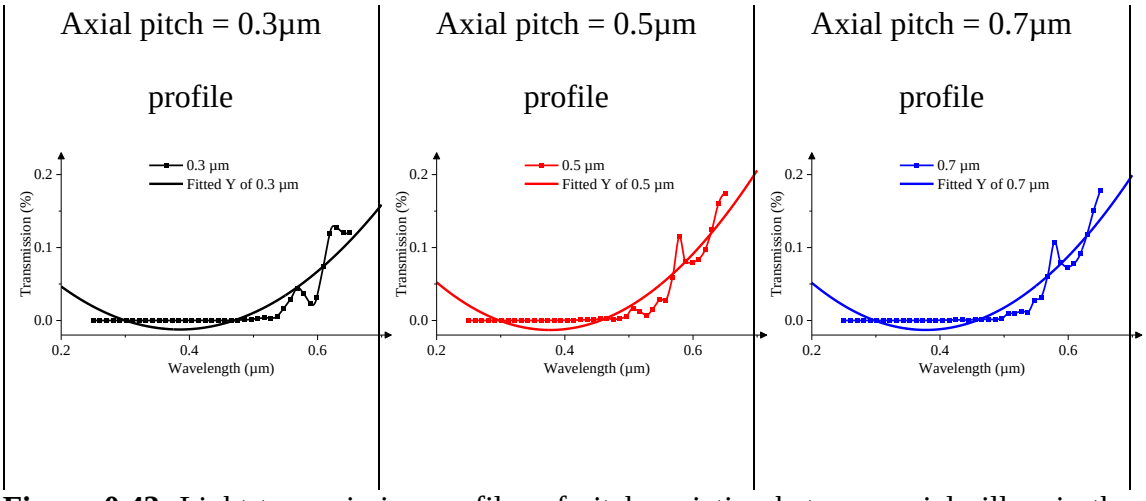

Figure 0.43: Light transmission profiles of pitch variation between axial pillars in the range of 0.3µm to 0.7µm for a ZnO/ZnTe micropillar solar cell.

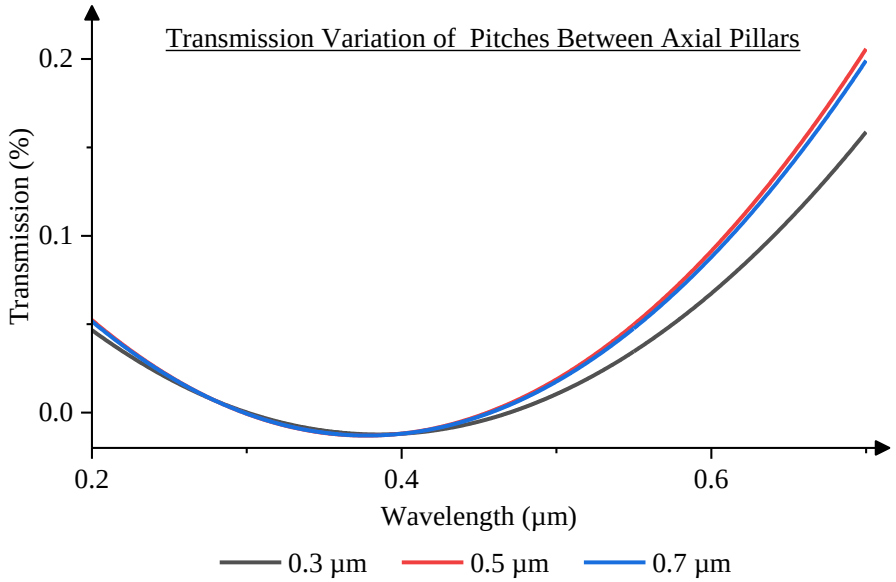

Figure 0.44: Comparative graph of light transmission percentage of three different radial pillar shell thickness of ZnO/ZnTe micropillar solar cell.

Reflection profiles of pitch between axial pillars

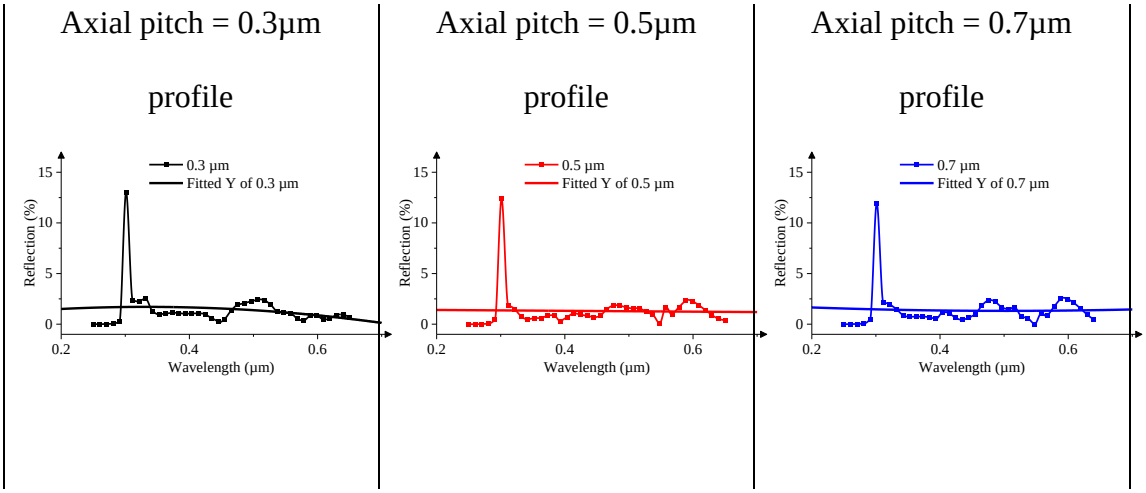

Figure 0.45: Light reflection profiles of pitch variation between axial pillars in the range of 0.3μm to 0.7μm for a ZnO/ZnTe micropillar solar cell.

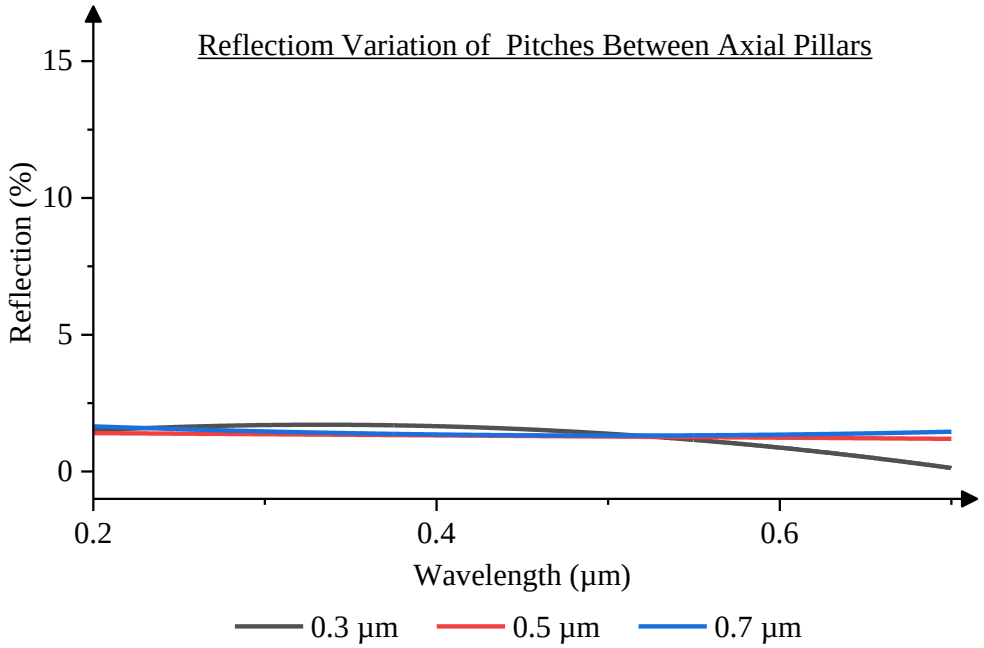

Figure 0.46: Comparative graph of light reflection percentage of three different pitches between pillars of axial junction ZnO/ZnTe micropillar solar cell.

Absorption profiles of pitch between axial pillars

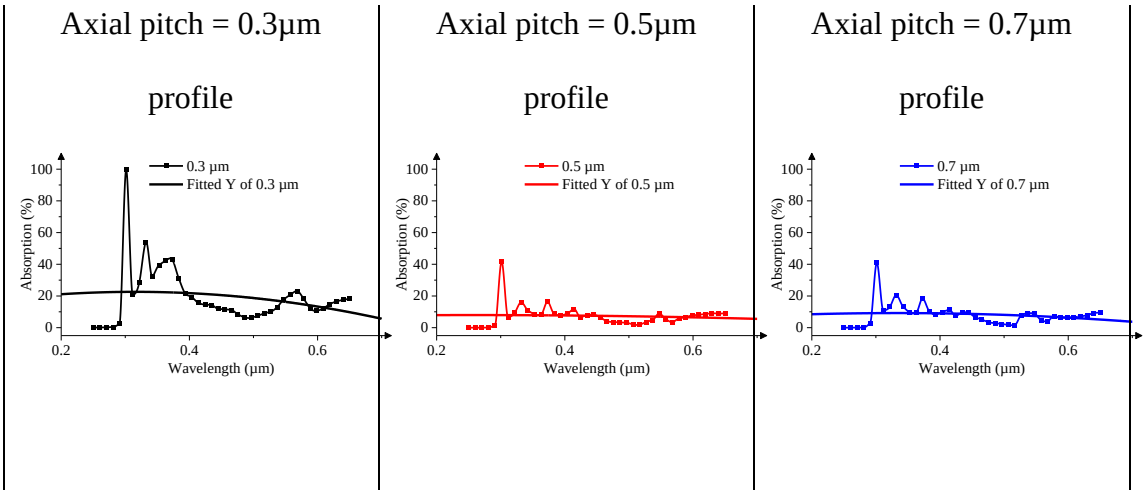

Figure 0.47: Light absorption profiles of pitch variation between axial pillars in the range of 0.3µm to 0.7µm for a ZnO/ZnTe micropillar solar cell.

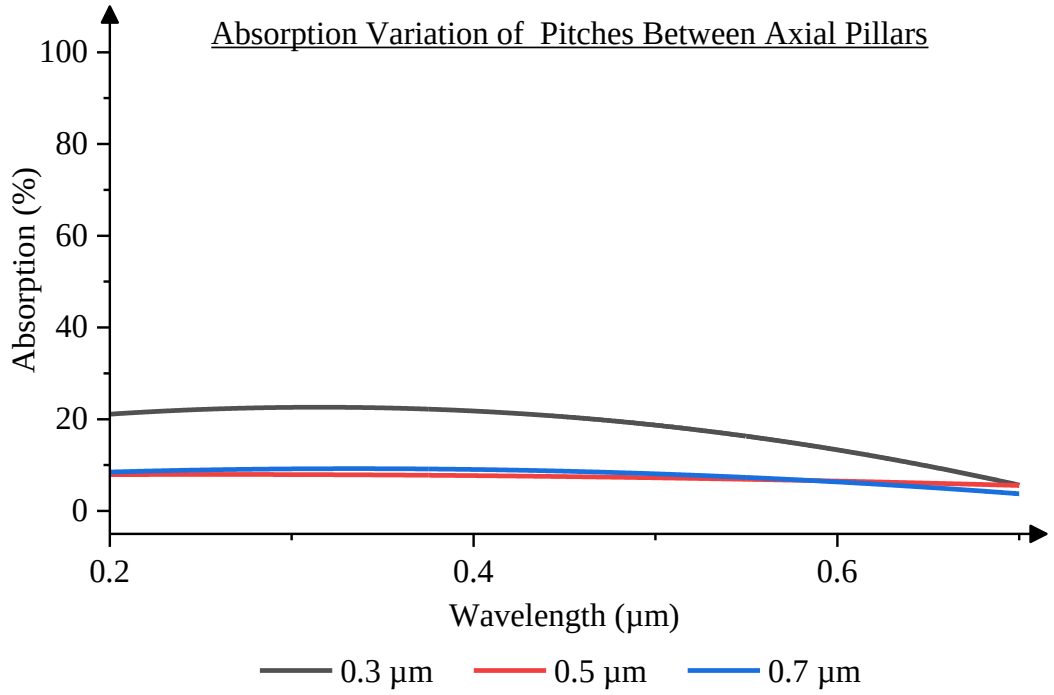

Figure 0.48: Comparative graph of light reflection percentage of three different pitches between pillars of axial junction ZnO/ZnTe micropillar solar cell.

Axial Pillars Pitch Variation Analysis

The lowest pitch of 0.3 µm (black colour) with a very tight spacing between two neighbouring pillars causes high light reflection as shown in Figure 4.46 and light absorption as shown in Figure 4.48. For each of the three variations (0.3 µm, 0.5 µm, and 0.7 µm), the absorption spectrum throughout the full wavelength is less than thirty percent (30%). This makes it very obvious that light doesn't get caught between the pillars but merely reflects off the surface. On the other hand, for the majority of the wavelength range, the maximum pitch value of 0.7 µm (which is indicated as blue in the figures) exhibits lesser reflection and absorption. Figure 4.44 exhibits very low transmission values of less than three percent (3%).

4.4.2 Radial Pillars Pitch Changing Effect

In this part, the impact of the pitch between neighbouring radial pillars in the range of 0.3 µm ~ 0.7 µm is investigated while maintaining the fixed values of the pillar height and diameter/thickness at 1.5 µm and 200 nm, respectively. The three pitches that were taken into consideration for this simulation were 0.3 µm (marked in black), 0.5 µm (marked in red), and 0.7 µm (marked in blue). Figure 4.49 ~ Figure 4.54 shows the transmission, reflection, and absorption profile as a function of the distance between two neighbouring pillars.

Transmission profiles of pitch between radial pillars

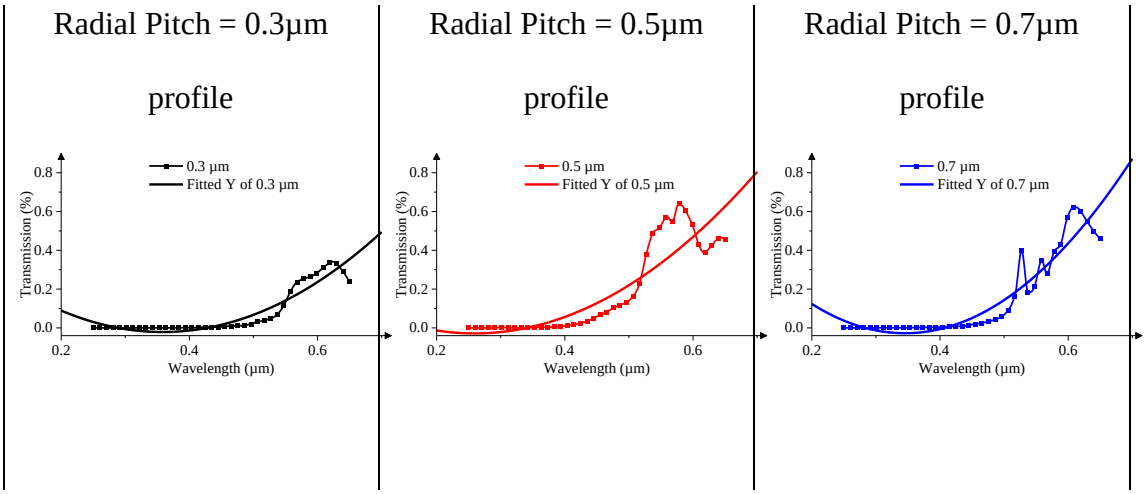

Figure 0.49: Light transmission profiles of pitch variation between radial (core-shell) pillars in the range of 0.3µm to 0.7µm for a ZnO/ZnTe micropillar solar cell.

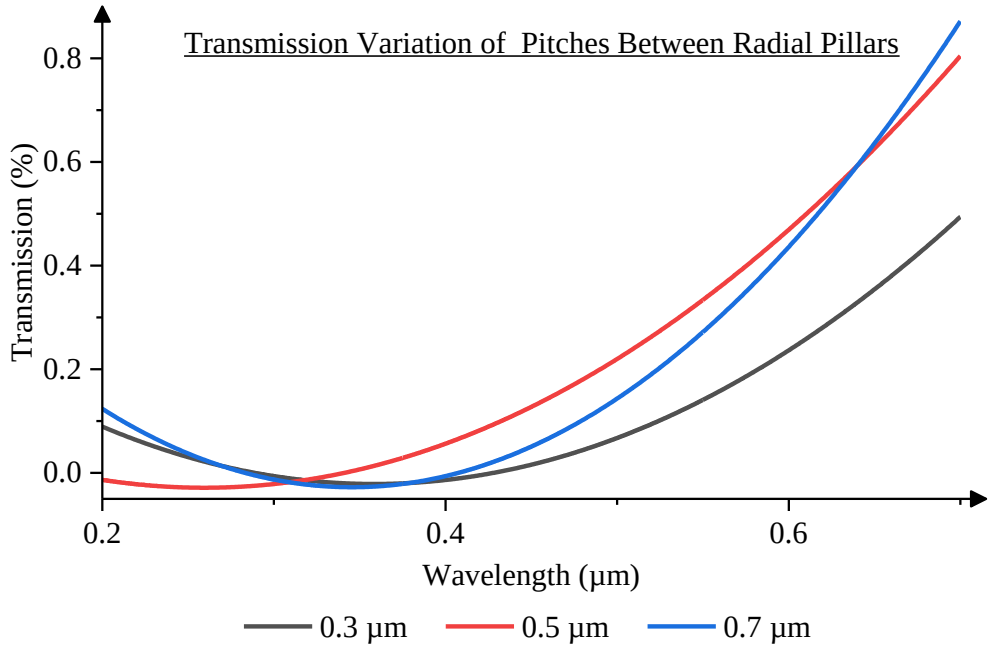

Figure 0.50: Comparative graph of light transmission percentage of three different pitches between pillars of radial junction ZnO/ZnTe micropillar solar cell.

Reflection profiles of pitch between radial pillars

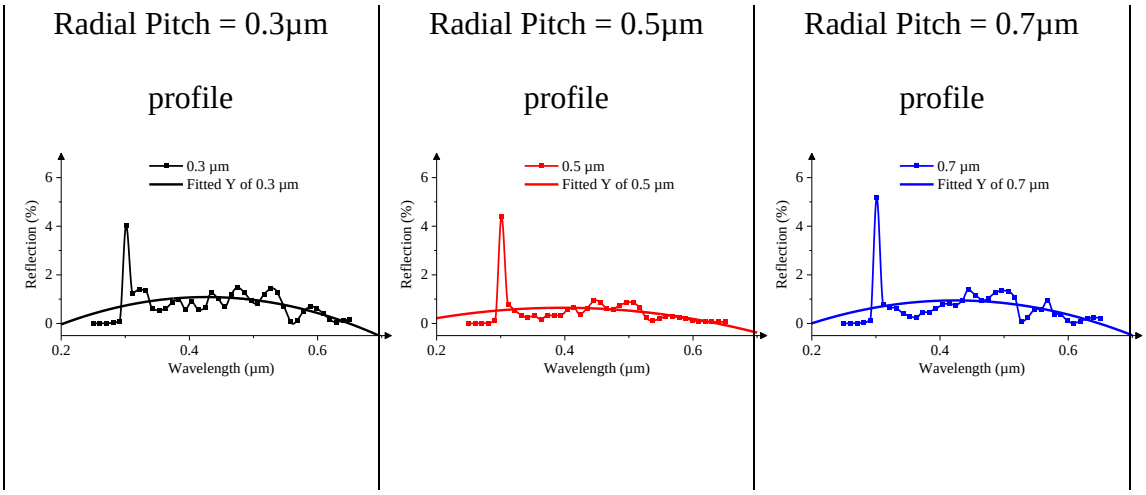

Figure 0.51: Light reflection profiles of pitch variation between radial (core-shell) pillars in the range of 0.3µm to 0.7µm for a ZnO/ZnTe micropillar solar cell.

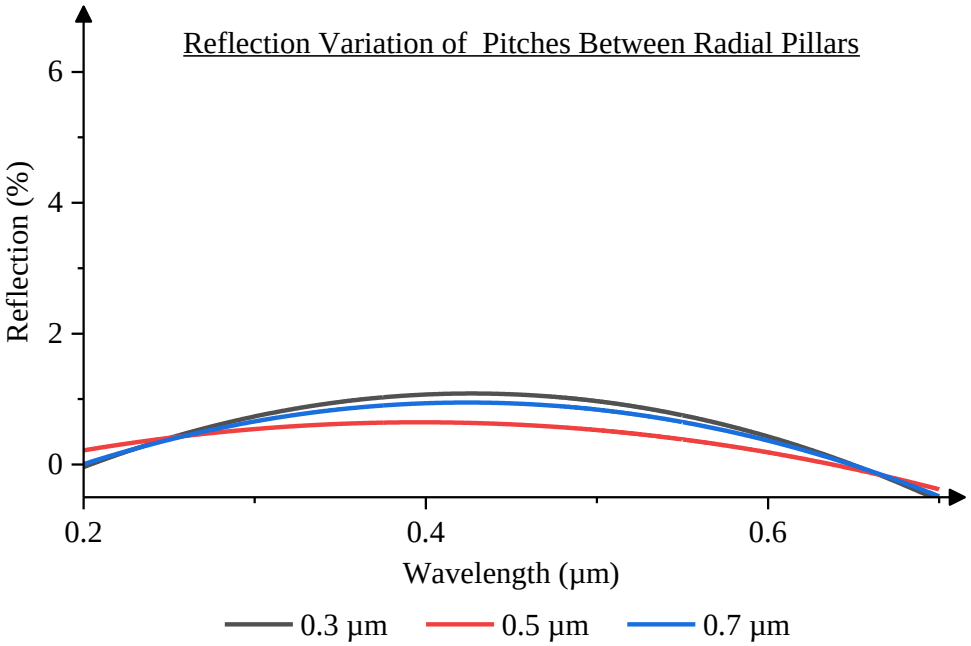

Figure 0.52: Comparative graph of light reflection percentage of three different pitches between pillars of radial junction ZnO/ZnTe micropillar solar cell.

Absorption profiles of pitch between radial pillars

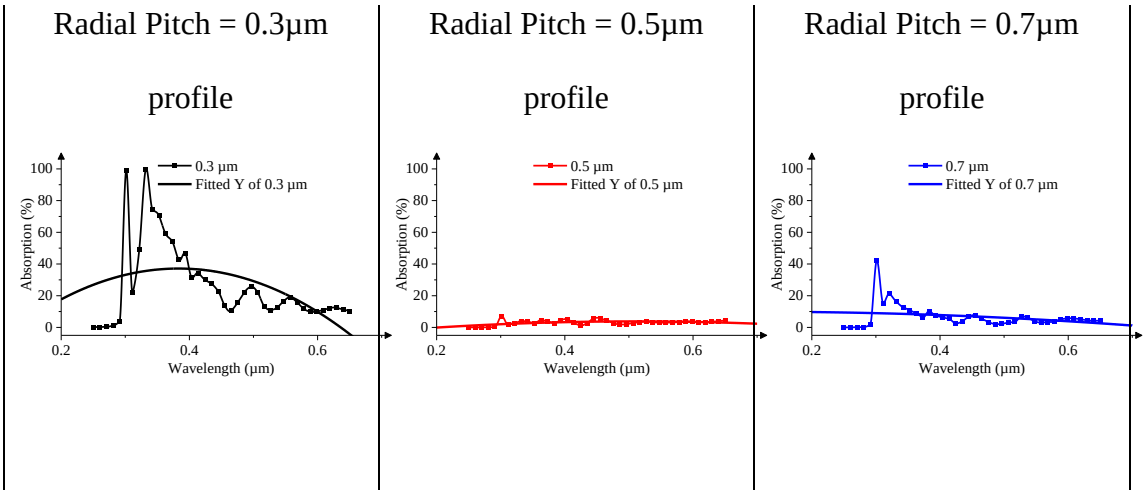

Figure 0.53: Light absorption profiles of pitch variation between radial (core-shell) pillars in the range of 0.3µm to 0.7µm for a ZnO/ZnTe micropillar solar cell.

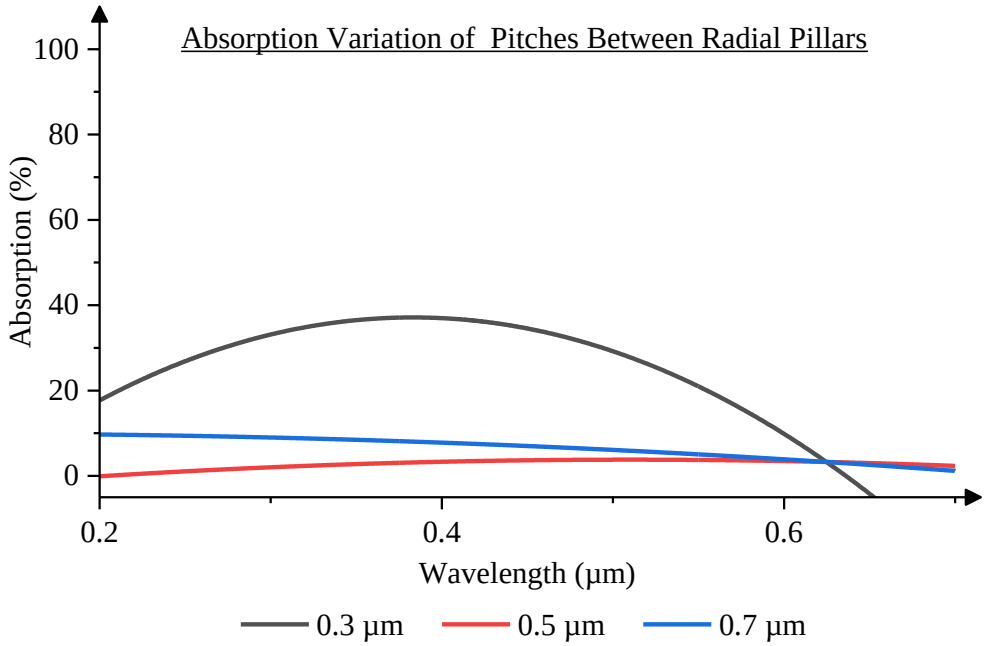

Figure 0.54: Comparative graph of light absorption percentage of three different pitches between pillars of radial junction ZnO/ZnTe micropillar solar cell.

Radial Pillars Pitch Variation Analysis

The highest optical performance is found at 0.3 µm among the three values of the radial pillar pitches (0.3 µm, 0.5 µm and 0.7 µm). It had the lowest light transmission and the largest light absorption, as illustrated in Figure 450 and Figure 4.54 in black. Additionally, Figure 4.50 and Figure 4.52 show that the 0.5 µm pitch had the maximum transmission and lowest reflection, respectively. Both 0.5 µm and 0.7 µm values exhibit a similar pattern of transmission, reflection, and absorption; of higher transmission but lower reflection and absorption.

4.5 Summary

The pillar height may be as big as necessary in line with the equation $H > 1/\alpha$, where H = length of the pillar / thickness of the absorber layer and $1/\alpha$ = optical length. Additionally, a rise in shell thickness eventually results in an increase in the creation of

carriers from the perspective of optical response. Thus, the collecting of all these carriers is the biggest challenge. In a radial (core-shell) junction solar cell, the directions of incident light and carrier collection are orthogonal. As a result, the radial p-n junction collects the carriers. This problem prevents the diameter of the shell from having a random thickness. In actuality, the device's optical performance is significantly impacted by the device's diameter to pitch ratio.

CHAPTER FIVE

CONCLUSION AND RECOMMENDATION

This chapter present summaries, conclusion and recommendation of this research and a future outlook.

5.1 Conclusion

Solar cells based on II-VI semiconductors are among the leading candidates for low-cost photovoltaic conversion of solar energy due to their high absorption and therefore the low material consumption for their production. This work reports on the analysis of negatively doped Zinc Oxide (ZnO) and positively doped Zinc Telluride (p-ZnTe) micropillar solar cells by using Finite-Difference Time-Domain (FDTD) Solver in the Ansys Lumerical DEVICE Simulator software. The simulation analysed different structures and optical properties (reflection, transmission, and absorption) as functions of several varying pillar dimension such as height, diameter and pitch.

The radial (core-shell) ZnO/ZnTe micropillar solar cell device outperforms the other two geometrical structures (axial micropillar and the planar ZnO/ZnTe solar cells). The results demonstrate lower reflection throughout the full wavelength and an increased absorption. The inclusion of micropillars into both axial and radial junction ZnO/ZnTe solar cells accounted for the improved optical performance over the planar ZnO/ZnTe solar cell.

Longer pillars allow more transmission, but minimizes reflection and absorption. The study findings indicates that, an axial pillar with a height of 1.5μm (with absorber height

of 1.0µm and emitter height of 0.5µm) and a radial (core-shell) pillar with a height of 1.3µm had the highest average absorption of forty percent (40%).

Findings also indicate that, thicker diameters offer more absorption in the 0.30µm to 0.55µm wavelength range as well as lowest reflection in axial structures but highest reflection in radial structures. Given these considerations, a pillar with a core diameter of 100nm and a shell thickness of 240nm will be beneficial. The optimal pitch for both axial and radial (core-shell) ZnO/ZnTe micropillar structures has been chosen to be 0.3µm, taking into account the percentage difference in absorption compared to the other two pitches (0.5µm and 0.7µm). However, the 0.5µm pitch value underperformed when compared to the higher 0.7µm pitch value. As a result, the pitch value must be determined between the two extreme values.

These results are useful for understanding solar cell devices as well as feedback for modelling high efficiency ZnO/ZnTe micropillar solar cells by designers and producers.

5.2 Potential Extensions

The contributions of this work may be expanded in a number of ways as interest in micropillar solar cells continues to rise. Proposed extensions and future work are described briefly below.

1. Electrical Analysis of ZnO/ZnTe Micropillar Solar Cells

   The ZnO/ZnTe micropillar solar cells' capacity to generate charge carriers, the amount of doping they will need, the amount of recombination they will undergo, and the current they will produce may all be predicted by further simulation. This may be achieved by adding the optical performance findings to the CHARGE solver of the Ansys Lumerical application.

2. Analysis of ZnO/ZnTe Solar Cells with Triangular Micropillars

Other types of micropillars, such as those that are triangular, conical, or rectangular in shape, can also be replicated as a variation on the pillar-type structure, which has a cylindrical geometry. These structures each have their own benefits and drawbacks. On the basis of the pillar geometry, it will be essential to select and specify the proper boundary conditions.

3. Analyzing the Effect of Radiative Recombination in ZnO/ZnTe Solar Cells

   In ZnO/ZnTe solar cell structures, auger, radiative, and shockleyread-hall recombination may be observed. Investigating the severity and relevance of these phenomena in affecting the performance of solar cells would make for an intriguing future research.

REFERENCE

Akram, M. A., Javed, S., Islam, M., Mujahid, M., & Safdar, A. (2016). Arrays of CZTS sensitized ZnO/ZnS and ZnO/ZnSe core/shell nanorods for liquid junction nanowire solar cells. *Solar Energy Materials and Solar Cells*, *146*, 121–128.

Baytemir, G., Ciftpinar, E. H., & Turan, R. (2019). Enhanced metal assisted etching method for high aspect ratio microstructures: Applications in silicon micropillar array solar cells. *Solar Energy*, *194*, 148–155.

Beek, W., Wienk, M., & Janssen, R. (2004). Efficient Hybrid Solar Cells from Zinc Oxide Nanoparticles and a Conjugated Polymer. *Advanced Materials*, *16*, 1009–1013. https://doi.org/10.1002/adma.200306659

Chao, H., Cheng, J., Lu, J., Chang, Y., Cheng, C., & Chen, Y. (2010). Growth and characterization of type-II ZnO/ZnTe core-shell nanowire arrays for solar cell applications. *Superlattices and Microstructures*, *47*(1), 160–164.

Chao, H., You, S., Lu, J., Cheng, J., Chang, Y., Liang, C.-T., & Wu, C. (2011). The Growth and Characterization of ZnO/ZnTe Core–Shell Nanowires and the Electrical Properties of ZnO/ZnTe Core–Shell Nanowire Field Effect Transistor. *Journal of Nanoscience and Nanotechnology*, *11*(3), 2042–2046.

Dhar, A., Pradhan, D., & Roy, J. (2016). *Nanostructures for highly efficient ultra-thin silicon solar cells*. 1–5.

Fan, J. C., Sreekanth, K., Xie, Z., Chang, S., & Rao, K. V. (2013). p-Type ZnO materials: Theory, growth, properties and devices. *Progress in Materials Science*, *58*(6), 874–985.

Fan, Z., Razavi, H., Do, J., Moriwaki, A., Ergen, O., Chueh, Y.-L., Leu, P. W., Ho, J. C., Takahashi, T., & Reichertz, L. A. (2009). Three-dimensional nanopillar-array photovoltaics on low-cost and flexible substrates. *Nature Materials*, *8*(8), 648–653.

Fang, F., McCandless, B., & Opila, R. (2009). *Chemical and electrical properties of ZnTe based solar cells*. 001258–001263.

Garnett, E. C., Brongersma, M. L., Cui, Y., & McGehee, M. D. (2011). Nanowire solar cells. *Annual Review of Materials Research*, *41*(1), 269–295.

Garnett, E., & Yang, P. (2010). Light trapping in silicon nanowire solar cells. *Nano Letters*, *10*(3), 1082–1087.

Gessert, T., Mason, A., Reedy, R., Matson, R., Coutts, T., & Sheldon, P. (1995). Development of rf sputtered, Cu-doped ZnTe for use as a contact interface layer to p-CdTe. *Journal of Electronic Materials*, *24*(10), 1443–1449.

Gharghi, M., Fathi, E., Kante, B., Sivoththaman, S., & Zhang, X. (2012). Heterojunction silicon microwire solar cells. *Nano Letters*, *12*(12), 6278–6282.

Goel, S., Sinha, N., Yadav, H., Joseph, A. J., & Kumar, B. (2017). Experimental investigation on the structural, dielectric, ferroelectric and piezoelectric properties of La doped ZnO nanoparticles and their application in dye-sensitized solar cells. *Physica E: Low-Dimensional Systems and Nanostructures*, *91*, 72–81.

Greulich, J., Fellmeth, T., Glatthaar, M., Biro, D., & Rein, S. (2012). Comparison of analytical and numerical models for the optimization of c-Si solar cells' front metallization. *IEEE Journal of Photovoltaics*, *2*(4), 588–591.

Han, D.-H., Choi, S.-J., & Park, S.-M. (2003). Electrochemical preparation of zinc telluride films on gold electrodes. *Journal of The Electrochemical Society*, *150*(5), C342.

Jouane, Y., Colis, S., Schmerber, G., Kern, P., Dinia, A., Heiser, T., & Chapuis, Y.-A. (2011). Room temperature ZnO growth by rf magnetron sputtering on top of photoactive P3HT: PCBM for organic solar cells. *Journal of Materials Chemistry*, *21*(6), 1953–1958.

Kabalan, A., & Sohid, S. B. (2020). Optical and Electrical Analysis of Core-Shell ZnO/ZnTe Micropillar Solar Cells. *IEEE Journal of the Electron Devices Society*, *8*, 701–710.

Kelzenberg, M. D., Boettcher, S. W., Petykiewicz, J. A., Turner-Evans, D. B., Putnam, M. C., Warren, E. L., Spurgeon, J. M., Briggs, R. M., Lewis, N. S., & Atwater, H. A. (2010). Enhanced absorption and carrier collection in Si wire arrays for photovoltaic applications. *Nature Materials*, *9*(3), 239–244.

Lanjewar, M., & Gohel, J. V. (2017). Enhanced performance of Ag-doped ZnO and pure ZnO thin films DSSCs prepared by sol-gel spin coating. *Inorganic and Nano-Metal Chemistry*, *47*(7), 1090–1096.

Leschkies, K. S., Beatty, T. J., Kang, M. S., Norris, D. J., & Aydil, E. S. (2009). Solar cells based on junctions between colloidal PbSe nanocrystals and thin ZnO films. *ACS Nano*, *3*(11), 3638–3648.

Li, L., Zhai, T., Bando, Y., & Golberg, D. (2012). Recent progress of one-dimensional ZnO nanostructured solar cells. *Nano Energy*, *1*(1), 91–106.

Li, S.-S., & Chen, C.-W. (2013). Polymer–metal-oxide hybrid solar cells. *Journal of Materials Chemistry A*, *1*(36), 10574–10591.

Liao, Y. X., & Yi, F. T. (2009). *Simulation of the Optical Properties for Silicon Nano-pillar Array using Finite Difference Time Domain Method*. *60*, 367–370.

Liu, K., Sakurai, M., & Aono, M. (2010). ZnO-based ultraviolet photodetectors. *Sensors*, *10*(9), 8604–8634.

Lumerical, A. (2019). *Lumerical scripting language—Alphabetical list*. Lumerical Support. https://support.lumerical.com/hc/en-us/articles/360034923553-Lumerical-scripting-language-Alphabetical-list

Luo, S., He, X., Shen, H., Li, J., Yin, X., Oron, D., & Lin, H. (2017). Vertically aligned ZnO/ZnTe core/shell heterostructures on an AZO substrate for improved photovoltaic performance. *RSC Advances, 7*(24), 14837–14845.

Mahmood, K., & Park, S. B. (2013). Highly efficient dye-sensitized solar cell with an electrostatic spray deposited upright-standing boron-doped ZnO (BZO) nanoporous nanosheet-based photoanode. *Journal of Materials Chemistry A, 1*(15), 4826–4835.

Mariani, G., Haddad, M., Rajagopal, A., & Huffaker, D. L. (2022). *High-efficiency nanopillar solar cells employing wide-bandgap surface recombination barriers*.

McCandless, B. E., & Dobson, K. D. (2004). Processing options for CdTe thin film solar cells. *Solar Energy*, *77*(6), 839–856.

Michallon, J., Bucci, D., Morand, A., Zanuccoli, M., Consonni, V., & Kaminski-Cachopo, A. (2014). Light trapping in ZnO nanowire arrays covered with an absorbing shell for solar cells. *Optics Express*, *22*(104), A1174–A1189.

Nations, U. (2022). *What is renewable energy?* United Nations; United Nations. https://www.un.org/en/climatechange/what-is-renewable-energy

NREL. (2019). *Best Research-Cell Efficiency Chart*. National Renewable Energy Laboratory. https://www.nrel.gov/pv/cell-efficiency.html

Olson, D. C., Piris, J., Collins, R. T., Shaheen, S. E., & Ginley, D. S. (2006). Hybrid photovoltaic devices of polymer and ZnO nanofiber composites. *Thin Solid Films, 496*(1), 26–29.

Pistone, A., Arico, A., Antonucci, P., Silvestro, D., & Antonucci, V. (1998). Preparation and characterization of thin film ZnCuTe semiconductors. *Solar Energy Materials and Solar Cells*, *53*(3–4), 255–267.

Sahoo, M. K., & Kale, P. (2019). Integration of silicon nanowires in solar cell structure for efficiency enhancement: A review. *Journal of Materiomics*, *5*(1), 34–48.

Sakai, N., Usui, R., & Murakami, T. N. (2013). Optimum particle size of ZnO for dye-sensitized solar cells. *Chemistry Letters*, *42*(8), 810–812.

Schrier, J., Demchenko, D. O., & Alivisatos, A. P. (2007). Optical properties of ZnO/ZnS and ZnO/ZnTe heterostructures for photovoltaic applications. *Nano Letters*, *7*(8), 2377–2382.

Sellai, A. (2013). *Enhancement of light absorption in thin film solar cells with metallic nano-strips*. 298–302.

Shaygan, M., Davami, K., Jin, B., Gemming, T., Lee, J.-S., & Meyyappan, M. (2016). Highly sensitive photodetectors using ZnTe/ZnO core/shell nanowire field effect transistors with a tunable core/shell ratio. *Journal of Materials Chemistry C*, *4*(10), 2040–2046.

Shieh, J., You, C. Y., Liu, J. M., & Chiu, C. C. (2016). *Improving optical and electrical properties of micropillar and black-Si solar cells by combining them into a superstructure*. 222–224.

Sites, J., & Pan, J. (2007). Strategies to increase CdTe solar-cell voltage. *Thin Solid Films*, *515*(15), 6099–6102.

Skhouni, O., El Manouni, A., Mari, B., & Ullah, H. (2016). Numerical study of the influence of ZnTe thickness on CdS/ZnTe solar cell performance. *The European Physical Journal Applied Physics*, *74*(2), 24602.

Strevel, N., Trippel, L., Kotarba, C., & Khan, I. (2013). Improvements in CdTe module reliability and long-term degradation through advances in construction and device innovation. *Photovoltaics International*, *22*, 66–74.

Takanezawa, K., Hirota, K., Wei, Q.-S., Tajima, K., & Hashimoto, K. (2007). Efficient charge collection with ZnO nanorod array in hybrid photovoltaic devices. *The Journal of Physical Chemistry C*, *111*(19), 7218–7223.

Tanaka, T., Miyabara, M., Saito, K., Guo, Q. X., Nishio, M., Yu, K. M., & Walukiewicz, W. (2013). *Development of ZnTe-based solar cells*. *750*, 80–83.

Tiwari, G. N., & Mishra, R. K. (2012). *Advanced renewable energy sources*. Royal Society of Chemistry.

Trusted Photonic Simulation Tools—About Lumerical. (2022). Lumerical. https://www.lumerical.com/about-lumerical/

UNFCC. (2015). *Adoption of the Paris Agreement*. FCCC/CP/2015/L. 9/Rev. 1.

Wang, W., Feng, Q., Jiang, K., Huang, J., Zhang, X., Song, W., & Tan, R. (2011). Dependence of aluminum-doped zinc oxide work function on surface cleaning method as studied by ultraviolet and X-ray photoelectron spectroscopies. *Applied Surface Science*, *257*(9), 3884–3887.

Wang, W., Lin, A., & Phillips, J. (2008). Electrical characteristics and photoresponse of ZnO/ZnTe heterojunction diodes. *Journal of Electronic Materials*, *37*(8), 1044–1048.

WBGU. (2003). *World in Transition 3: Towards Sustainable Energy Systems*. Routledge.

Wibowo, A., Marsudi, M. A., Amal, M. I., Ananda, M. B., Stephanie, R., Ardy, H., & Diguna, L. J. (2020). ZnO nanostructured materials for emerging solar cell applications. *RSC Advances*, *10*(70), 42838–42859.

Xu, J., Lee, S. H., Bell, Z. W., Smith, B., Zhang, X.-G., Ju, T., Chen, A.-J., & Pan, Z. (2010). *Study of charge transport mechanisms in ZnO-ZnTe nanojunctions*. *7805*, 199–205.

Zang, Z. (2018). Efficiency enhancement of ZnO/Cu2O solar cells with well oriented and micrometer grain sized Cu2O films. *Applied Physics Letters*, *112*(4), 042106.

Zhang, Y., Fan, Z., Zhang, W., Ma, Q., Jiang, Z., & Ma, D. (2018). High performance hybrid silicon micropillar solar cell based on light trapping characteristics of Cu nanoparticles. *AIP Advances*, *8*(5), 055309.